Probabilistic Turbine Blade Thermal Analysis of Manufacturing Variability and Toleranced Designs

by

Curtis William Moeckel

Submitted to the Department of Aeronautics and Astronautics
in partial fulfillment of the requirements for the degree of

Master of Science in Aeronautics and Astronautics

at the

MASSACHUSETTS INSTITUTE OF TECHNOLOGY

January 2006

Author .....
Department of Aeronautics and Astronautics
January 30, 2006

Certified by .....
David L. Darmofal
Associate Professor of Aeronautics and Astronautics, MacVicar Fellow
Thesis Supervisor

Accepted by .....
Jaime Peraire
Professor of Aeronautics and Astronautics
Chair, Committee on Graduate Students

Probabilistic Turbine Blade Thermal Analysis of Manufacturing Variability and Toleranced Designs

by

Curtis William Moeckel

Submitted to the Department of Aeronautics and Astronautics
on January 30, 2006, in partial fulfillment of the
requirements for the degree of
Master of Science in Aeronautics and Astronautics

Abstract

Manufacturing variability is likely the primary cause of a large scatter in the life of gas turbine hot-section components. This research deals with schemes to improve robustness through tolerancing input parameters in ranges of the distributions which make non-conformances more likely. The need for probabilistic analysis to investigate this problem is substantiated due to differences which arise when input parameters vary at different levels, for example the engine-to-engine and blade-to-blade level. Specifically, the importance of blade-to-blade level input parameters relative to engine-to-engine level input parameters becomes increasingly important for larger numbers of blades in a row. A framework for calculating the potential number of prevented non-conformances and the corresponding cost savings associated with various tolerancing schemes is presented.

Specifically this research investigates manufacturing variability and its effect on first-stage turbine blades through the use of a parametric CAD model, automated CAD regeneration software, and a parametric finite element thermal model. Probabilistic analysis is performed using Monte Carlo simulation on both the finite element model as well as response surfaces built from the finite element model. Blade-to-blade cooling flow variability, especially as a result of film-hole diameter variability in critical locations is identified as the most likely candidate for parameter tolerancing. More promising is a combined two-factor tolerancing scheme which additionally tolerances gas path temperature.

Thesis Supervisor: David L. Darmofal
Title: Associate Professor of Aeronautics and Astronautics, MacVicar Fellow

Acknowledgments

An aeronautical engineer is forever indebted to the first person to take him to an airshow. More than taking me to see The Blue Angels and humoring the "do you think it could fly?" question accompanying hundreds of airplane sketches, my father has been the one to peak my interest, guide my decisions, and explain the marvel that is turbomachinery. I would also like to thank my mother for all that she has done for me. Her selflessness and encouragement has helped me overcome many challenges.

For the foundation of my engineering education, I am indebted to Mr. Garrison, Professor Kelly, and Professor Krier. For real-world guidance I am indebted to Roger Paollilo, Dave Cloud, Ferry DeJong, Chester Wang, Leo Chuzhoy, Howard Becker, Ed Zurmehly, Chi-Fai Chan, Mike McNamee, Jeff Guymon, Jim Hadder, John Crawford, and many others along the way.

Directly related to the contents of this thesis, I am indebted to Bob Haimes and Ali Merchant for creating and supporting CAPRI, David Walfisch for creating the parametric CAD model with his UniGraphics expertise, Rob Kingston, Rob Norton, and Alexander Karl for their technical correspondence and guidance, and most of all Professor Darmofal. Professor Darmofal has been my strongest influence and greatest ally toward furthering my education. His patient advice has proved invaluable in guiding this research while maximizing my learning opportunities.

The support to attend MIT is the greatest gift I have ever received. Thank you Rolls-Royce for establishing and supporting the Whittle Fellowship. Your gift extends beyond my education and this research, for without this opportunity to attend MIT, I would have never met the love of my life. Siri, your patience, love, and support is worth more than you will ever know. And finally, thanks to Ed Lefren for demonstrating to me that the responsibility of an engineer is something which should never be taken lightly.

Contents

List of Figures

List of Tables

Chapter 1

Introduction

1.1 Motivation

Modern turbofan engines have improved upon the original turbojet designs of Sir Frank Whittle and Dr. Hans von Ohain through a continual increase in turbine rotor inlet temperature. This increase in temperature quickly necessitated that active cooling designs be considered for several hot-section components, including the first-stage turbine blade. Figure 1-1 [1] shows a cross section of a modern turbofan engine in which the first-stage turbine blade is cooled using air at a lower temperature from the high pressure compressor. The first-stage turbine blades are often referred to as "the heart of the engine" since their condition is critical to the engine as a system. Industry experience has demonstrated that non-conformances of first-stage turbine blades are one of the most common reasons for early engine removal and a major contributor to engine maintenance costs [2].

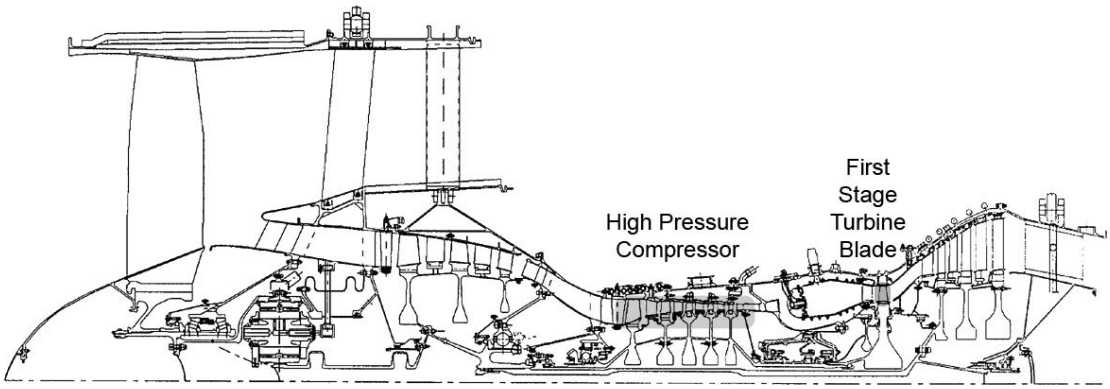

Figure 1-1: Cross section of a commercial turbofan (courtesy of SAE).

The historic increase in turbine rotor inlet temperature, seen in Figure 1-2, is a direct result of attempts to concurrently increase thermal efficiency and thrust per unit mass of air flow. The trend of increasing turbine rotor inlet temperature has continued past the data included in Figure 1-2 [3] such that most recent engines have turbine rotor inlet temperatures in excess of 1700 K (2600^{o}F).

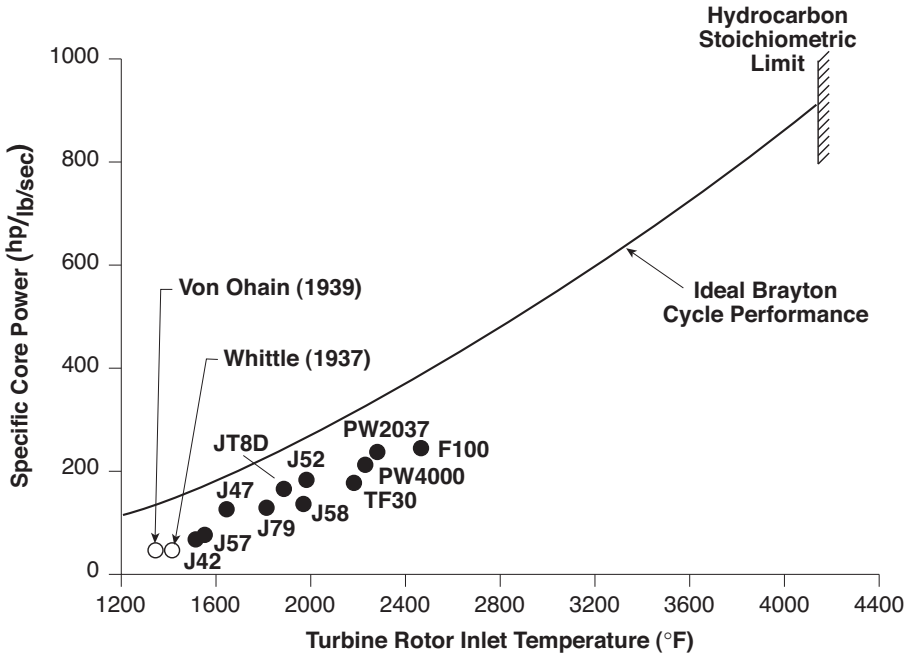

Figure 1-2: Historical trend of increasing turbine rotor inlet temperature (following Koff).

The adverse environment of ever-increasing severity in which first-stage turbine blades operate has required the introduction and continual-research into better materials and more effective cooling schemes. Materials have seen an approximately 275 K increase in acceptable operating temperature in the last 50 years. This is attributed to the development of nickel superalloys, and improvements in grain structure (equiaxed, directionally solidified, and single crystal). The last 20 years has also seen considerable progress in the development of ceramic thermal barrier coatings, which have found applications in turbine vanes and blades [4]. Improvements in cooling schemes have seen similar improvements as shown historically in Figure 1-3 [5]. Simple blade cooling was first introduced in the late 1950s and has progressed such that now convection, film, impingement, and transpiration cooling techniques are all available to the designer. Current designs will often use a combination of cooling techniques in a single blade (e.g. combined convection and film cooling).

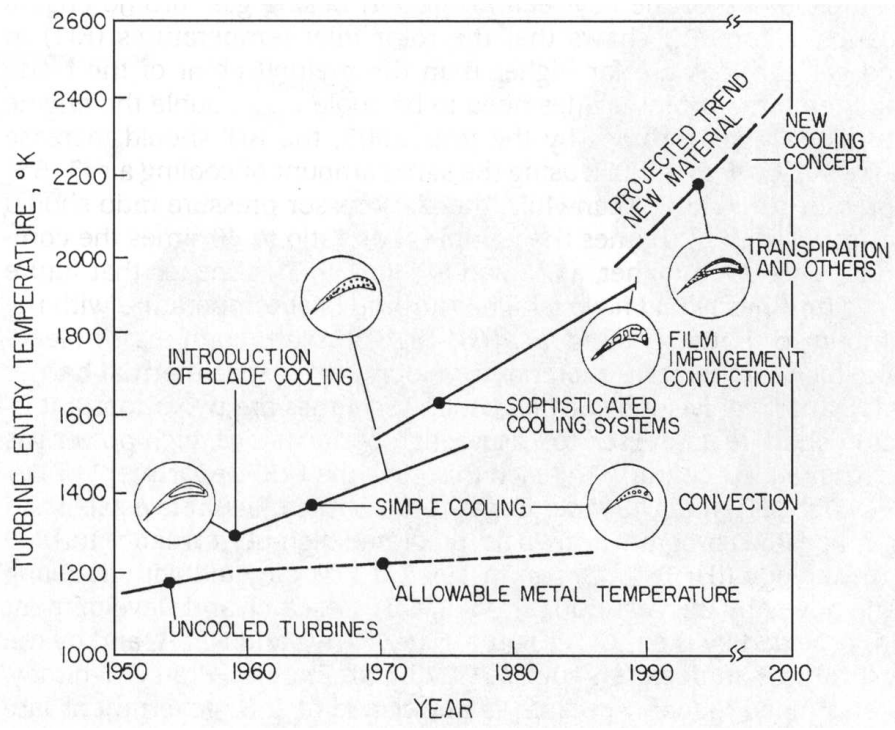

Figure 1-3: Advancements in cooling technology with time (courtesy of J.C. Han).

Despite substantial progress in materials and cooling technology, the benefits of increasing turbine rotor inlet temperature has continually challenged the technology. As a result, first-stage turbine blades have traditionally been designed to operate with little margin relative to numerous criteria which may cause a non-conforming blade.

A first-stage turbine blade may non-conform in the field for a variety of reasons, including thermo-mechanical fatigue (TMF)/low cycle fatigue (LCF), high cycle fatigue (HCF), creep, and environmental fatigue mechanisms including oxidation and corrosion. TMF/LCF is a fatigue mechanism which begins with a finite life until crack initiation followed by a finite life until the crack has propagated to an unacceptable extent. TMF/LCF is usually associated with engine accelerations/decelerations which cause transient thermal/mechanical stresses to occur either once or several times (depending on mission) per engine cycle. HCF is a fatigue mechanism whereby dynamical stresses (e.g. blade vibration) cycle the part a large number of times during each engine cycle. HCF life is similarly calculated by summing crack initiation and crack propagation life. The next mechanism is creep, a deformation phenomenon which occurs under load at high temperature. Creep life considers the number of operation hours at each power setting before the blade either deforms to an unaccept-

able extent or creep rupture occurs. Finally, environmental fatigue is a result of diffusion processes due to operating extended periods of time at high temperature. Like creep life, oxidation/corrosion life considers the number of allowable hours at each power setting before a non-conforming feature will emerge. In addition to having to consider multiple possible mechanisms leading to non-conformances, it should be noted that life can be highly non-linear with respect to assumed loads. Also, the problem is even more complex since various failure mechanisms tend to interact with each other [6]. For example, a blade which is undergoing creep deformation in the field will not have the same low cycle fatigue life as a blade which is not susceptible to creep.

The detection and replacement of non-conforming first-stage turbine blades is a topic which engine manufacturers have immense experience and knowledge, yet little is publicly disclosed since the information is of critical proprietary business importance. What is known is that the health of engines is monitored at three different levels. First, engine monitoring during operation on-wing allows for the detection of problems in high pressure turbines. Damage to a first-stage blade can cause less than desired work to be extracted by the turbine. If nothing were done, the high pressure rotor speed *N2* would drop. If a given engine pressure ratio *EPR* is required, more fuel would be required which would raise the exhaust gas temperature EGT [7] signaling a problem in the engine. The second level of monitoring first-stage turbine blades involves inspecting an on-wing engine on the ground. Using borescope inspection, if damage is apparent on even a single blade, the engine is removed from the airplane and sent for repair [2]. The final level at which first-stage turbine blades are inspected is as the individual pieces of a set which are removed from an engine during repair/overhaul. While there are some situations in which a repair is possible, a non-conformance of even a single blade can mandate that the entire set be replaced [8].

The need for first-stage turbine blades to perform robustly is more important now than ever. With the introduction of "power-by-the-hour" and TotalCare$^{\mathrm{TM}}$ [9] contracts, the manufacturer has assumed more responsibility for providing reliable power. In order to provide reliable power, turbine blade life must exhibit minimal scatter from part-to-part and the life-limiting blade must have a predictable and acceptable life, such that maintenance can be anticipated. Since an engine manufacturer may be in a situation where the same design is sold as both "power-by-the-hour" and traditional warranty-covered outright purchase, a

conservative design which substantially outlasts anticipated replacement intervals is not an acceptable business solution. The engineer is left with the burden of designing a robust blade which lasts at least to a predetermined replacement time with minimal scatter in life. This burden dictates that the engineer transition from a deterministic to a probabilistic design philosophy.

1.2 Thesis Objectives

The modeling requirements to predict the life of a turbine blade considering each failure regime is beyond the scope of this project. However, the computational expense of probabilistically predicting the temperature distribution of each blade within a fleet of engines is feasible even with modest computing resources. By assuming that certain failure mechanisms can be traced back to temperature-related phenomenon within a blade, the problem is pared down to a level where investigations related to design robustness can be pursued. The main objectives of this thesis can be enumerated as:

- To develop parameterized thermal models of a cooled turbine blade including computationally-inexpensive one-dimensional and computationally-manageable hybrid two-dimensional/three-dimensional models. These models will be utilized for probabilistic investigations.
- To develop a process for probabilistically ranking the effect of input parameters which enter the problem at different levels, e.g. engine-to-engine and blade-to-blade levels.
- To develop and evaluate computationally inexpensive techniques for understanding how changes in input parameters can affect the robustness of a design.
- To suggest and demonstrate ways in which controlling input parameters could lead to substantial robustness and cost benefits.

1.3 Project Approach

A representative (though hypothetical) convection and film-cooled first-stage turbine blade was provided by a turbine engine OEM (Rolls-Royce) as the baseline design for the project. Thermal solutions for the baseline configuration as well as one-factor at a time perturbations using proprietary Rolls-Royce software were also provided. The ANSYS finite element

package was then used to develop both a flow network and a thermal finite element model of the blade consisting of five planar sections connected with a flow network which could absorb heat from the blade metal.

The ANSYS flow network and thermal models were confirmed to respond similarly to the Rolls-Royce equivalents before proceeding. These parameterized ANSYS models were set up in such a way that the input variables could be assigned values at random from statistical distributions describing the variability in the input parameters. For physical geometric changes in the blade, a parameterized UniGraphics NX3 model (developed by David Walfisch of MIT) was created such that parameters like the core placement could be changed. The core placement and sectioning of each blade was handled in an automated fashion using CAPRI developed by Haimes [10].

In addition to the finite element model representation of the blade, various one dimensional resistance network models were pursued. The one dimensional models proved useful for capturing single outputs of the finite element model, e.g. average section temperature. With both the ANSYS finite element model as well as a one dimensional resistance model, response surface and Monte Carlo techniques were utilized to investigate the robustness of the baseline blade. The effect of input parameters were ranked and various means of controlling input parameters investigated. Finally, a tolerancing scheme was suggested and then explicitly modeled to demonstrate the potential for cost savings and robustness improvements to be made.

1.4 Contributions

Analyzing gas turbine hot section components in a probabilistic framework has been the topic of much previous research [11, 12, 13, 14, 6, 15]. The previous investigations will be built upon through the following unique contributions of this thesis:

- The first probabilistic finite element thermal analysis of a turbine blade including a parametric CAD master model allowing for core shift while also considering input parameters at both the blade-to-blade and the engine-to-engine level.
- Identification and ranking of key input parameters which affect the robustness of a first-stage turbine blade, even when those input parameters enter the problem at different levels, e.g. blade-to-blade and engine-to-engine.

- A novel method of controlling the tails of select input distributions with the effect of improving the robustness of first-stage turbine blades.
- A cost model which substantiates the potential for cost savings by pursuing robust first-stage turbine blades.

Chapter 2

Model Description

Thermal modeling of cooled turbine blades can range in fidelity from simple one-dimensional resistance-network models to complex conjugate heat transfer models [16]. In a probabilistic analysis, the fidelity of the models are limited by the computational expense of running a sufficient number of cases. The research will thus proceed with a simple one-dimensional model appropriate for rapidly developing and evaluating probabilistic techniques and a higher-fidelity finite element model. The finite element model shown in Figure 2-7 and discussed in detail in Section 2.3 consists of five planar sections of a convection and film cooled turbine blade coupled with external aerodynamic data and an internal flow network model. The one-dimensional model presented in Section 2.2 is designed to mimic the response of the finite element model but require significantly less computational expense.

2.1 Input Parameters

The first step of both deterministic and probabilistic analyses of the temperature distribution of a cooled gas turbine blade is to determine the key input parameters which might affect the temperature distribution in the part. In a deterministic analysis, an engineer will often chose one value for each of the input parameters which the model requires. If a risk is inherent, sensitivity analyses might also be performed to consider the range of input parameters considered to be critical. However, in a probabilistic framework, a differentiation between uncertainty and variability as well as the type of distribution and level at which the deviation occurs must be determined.

2.1.1 Uncertainty Versus Variability

There are two ways in which input parameters can differ from their single-value representations used in practice (e.g. mean, most-likely, assumed value). First, the uncertainty of a parameter can be characterized as the lack of knowledge relative to the true discrete value of each instance of the parameter. In contrast, the variability of a parameter is a measure of the range which the true discrete values of the parameter span for the population of interest.

In practice, some input parameters are inherently dominated by uncertainties while others are dominated by variabilities. Heat transfer coefficients are an example of an input parameter often dominated by uncertainty. Classical correlations, such as the Dittus-Boelter relation, may exhibit errors as large as 25%, while the complexity of more recent correlations can reduce the uncertainty to less than 10% [17]. In contrast, geometric features of a part are examples of parameters dominated by variability as a result of the manufacturing process. Using high precision measurement techniques (e.g. coordinate measuring machines) the variability of a feature from part-to-part is much greater than the uncertainty associated with the measurement.

When an engine only exists as a preliminary design, uncertainties are clearly of critical importance. Specifically for a cooled turbine blade, before the design is first tested in an engine, uncertainties on multiple input parameters can compound into an uncertainty of the design as a whole. If a cooled turbine blade design is deemed unsatisfactory in development as a result of an engine test, the manufacturer will generally have to do one or more of the following: redesign components, improve models and/or correlations, and possibly alter the development schedule. However, when a design is accepted as satisfactory and transitions into production, variabilities become of primary importance. If the production design is deemed unsatisfactory as a result of variability, the costs associated can include warranty claims, contractual costs, scrap, rework, redesign, and dissatisfied customers. Combining uncertainty and variability into the same analysis could lead to ambiguous conclusions, so the effects of each should be analyzed separately. The focus of this research will be on variability.

2.1.2 Parameter Level Classification

The levels at which parameters vary depends on how various units are grouped. For example, since each cooled turbine blade has a separate core around which the blade is formed, the deviation of the position of the core *core shift* is said to vary at the blade-to-blade level. That said, the tooling used to create the cores themselves may experience wear and have to be replaced or reworked after a certain number of batches. Thus wall thicknesses may have some variation at the blade batch-to-batch level. The recent research of Sidwell and Darmofal [2, 15], which demonstrated that blade-to-blade variability in cooling flow was a main driver of oxidation damage, highlights the importance of considering variability at the blade-to-blade level. Possible levels of variability can include the blade-to-blade, engine-to-engine, blade batch-to-batch, engine batch-to-batch, and airline-to-airline levels. The computational expense to study parameters can vary drastically depending on the level of variability which needs to be investigated. For this research, both blade-to-blade and engine-to-engine level variability will be investigated, requiring that each blade for every engine be separately modeled. Since a typical engine will include 70 cooled first stage turbine blades, even a minimal run of 500 engines will require 35,000 separate analyses.

2.1.3 Parameter Variability

Assigning variability to input parameters is a critical, yet often difficult step when performing probabilistic analysis. Data on each input parameter can be either limited in sample size, prohibitively expensive or impossible to obtain. Each parameter is generally described in a second moment context where mean μ and standard deviation σ are given for a distribution type, e.g. normal distribution. Statistical data sets were obtained for as many parameters as possible. For parameters not amenable to obtaining measured data, typical baseline values were used for the mean values and best estimates were made for the standard deviations [8, 18, 19].

The input parameters are presented in Tables 2.1 and 2.2 for the one-dimensional model and the finite element model, respectively. Statistical data sets for cycle parameters (69 engine data set) and bench check mass flow (487 blade data set) were used to form the distributions [20]. The parameters are grouped into one of three categories: engine-to-engine cycle parameters, blade-to-blade flow network parameters, and blade-to-blade conduction

parameters. Since this part is loosely based on industry experience, normalized values are presented. The manner in which these parameters will be used will be enumerated in Sections 2.2 and 2.3.

The parameter $\Delta RTDF_{engine}$ requires some explanation. Figure 2-1 shows typical values of T_0 at five locations along the span, the average which determines T_{41}. There is thus variability in the baseline inlet temperature with span: the lowest temperature is at the root, and the maximum is near mid-span. $\Delta RTDF_{engine}$ acts as a scaling parameter upon the difference between T_0 and T_{41} at each span, while keeping the same mean value for T_{41}.

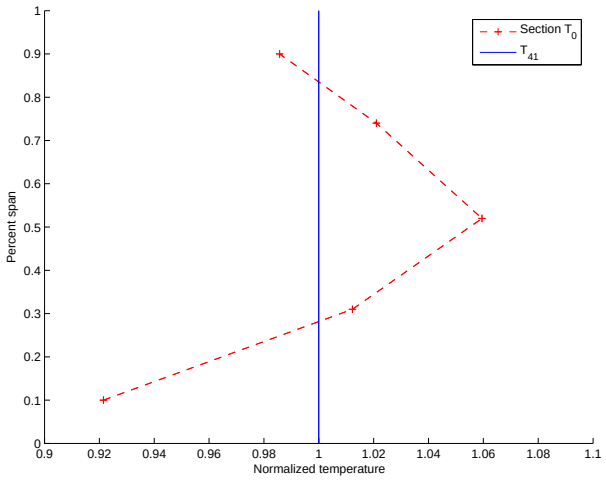

Figure 2-1: Typical radial temperature distribution function.

Also, it should be noted that variability in $\dot{m}_{cool,bench,blade}$ was available, but not the variability in input parameters to the flow solution which cause this variability. It will be assumed that all the holes in each row of film cooling have the same diameter and the variability in hole diameter for the different rows are independent, but have the same value of σ_D. With this assumption, the variability in film hole diameter is essentially due to misalignment of the blade and the hole-cutting device. A Monte Carlo technique was used to determine σ_D, such that the variability of the normalized $\sigma(\dot{m}_{cool,bench,blade})$=0.0244, as observed in the sample data.

Table 2.1: Input parameters which vary for one-dimensional model.

Engine-to-Engine Cycle Parameters				
Parameter	Nominal Value	Units	%(μ) 3σ Deviation	Lilliefors P-value
$T_{41,engine}$	1	normalized	1.47	0.137
$W_{41,engine}$	1	normalized	0.61	0.099
$T_{3,engine}$	0.42	normalized	0.88	>0.2

Blade-to-Blade Flow Network Parameter				
Parameter	Nominal Value	Units	%(μ) 3σ Deviation	Lilliefors P-value
$m_{cool,blade}$	1	normalized	7.31	0.040

Blade-to-Blade Conduction Parameters				
Parameter	Nominal Value	Units	%(μ) 3σ Deviation	Lilliefors P-value
$k_{sub,blade}$	1	normalized	10	N/A
$t_{sub,blade}$	1	normalized	10	N/A
$k_{tbc,blade}$	1	normalized	10	N/A
$t_{tbc,blade}$	1	normalized	20	N/A

Table 2.2: Input parameters which vary for finite element model.

Engine-to-Engine Cycle Parameters				
Parameter	Nominal Value	Units	%(μ) 3σ Deviation	Lilliefors P-value
$T_{41,engine}$	1	normalized	1.47	0.137
$\Delta RTDF_{,engine}$	$T_0(r)$-T_{41}	K	10	N/A
$W_{41,engine}$	1	normalized	0.61	0.099
$T_{3,engine}$	0.42	normalized	0.88	>0.2

Blade-to-Blade Flow Network Parameters				
Parameter	Nominal Value	Units	%(μ) 3σ Deviation	Lilliefors P-value
$m_{cool,blade*}$	1	normalized	7.31	0.040
$D_{SS,LE,blade}$	1	normalized	4.62	N/A
$D_{PS,LE,blade}$	1	normalized	4.62	N/A
$D_{PS,CN,blade}$	1	normalized	4.62	N/A
$D_{PS,TE,blade}$	1	normalized	4.62	N/A
*mass flow variability desired provided by variability in D_{films}				

Blade-to-Blade Conduction Parameters				
Parameter	Nominal Value	Units	%(μ) 3σ Deviation	Lilliefors P-value
$k_{sub,blade}$	1	normalized	10	N/A
$coreshift_{,blade*}$	0.0	N/A; 3σ=30% t_{wall}		N/A
$k_{tbc,blade}$	1	normalized	10	N/A
$t_{tbc,blade}$	1	normalized	20	N/A
* a positive value of core shift,blade corresponds to a thin PS				

The data was fit using the MATLAB Distribution Fitting Tool. This tool allows for a data set to be represented by a best fit continuous analytical distribution suitable for analysis. The Kolmogorov-Smirnoff test (K-S test) is a commonly used check to determine if a cumulative distribution function *CDF* fits a given data set. It was noted by Lilliefors [21] that the standard K-S tables are conservative to a type I error if one or more parameters must be estimated from the sample to be tested (as is the case in this research). Using Monte Carlo simulations, Lilliefors modified the K-S test to account for the uncertainty associated with estimating the mean and standard deviation from the sample data. Tables 2.1 and 2.2 give the p-value for those inputs for which data was available. The p-value is the probability of observing the given sample assuming that the population is normally distributed with mean and standard deviation given by the sample. The p-value of 0.04 for $\dot{m}_{cool,bench,blade}$ is somewhat low. However, the MATLAB Distribution Fitting Tool confirms that the normal distribution is the best standard distribution for the input, as well as $T_{41,engine}$, $W_{41,engine}$, and $T_{3,engine}$.

Another check to determine if it is appropriate to model a parameter as a continuous analytical distribution (e.g. normal) is to use graphical techniques, including histograms, cumulative distribution plots, and quantile-quantile plots. Figures 2-2 and 2-3 show both the comparison of the cumulative distribution and continuous fit as well as a quantile-quantile plot for best-fit normal distributions for turbine inlet temperature T_{41} and blade bench check mass flow $\dot{m}_{cool,bench,blade}$, respectively. For the cumulative distribution plots, good agreement is seen between the data set and the continuous analytical fit. The quantile-quantile plots better serve as a check of the tails of the distributions. It is clear, that there are some discrepancies between the data set for $\dot{m}_{cool,bench,blade}$ and the analytical fit in Figure 2-3b. However, in general, input variables showed approximately linear trends on a quantile-quantile plot, suggesting that modeling the distributions as normal is an acceptable assumption.

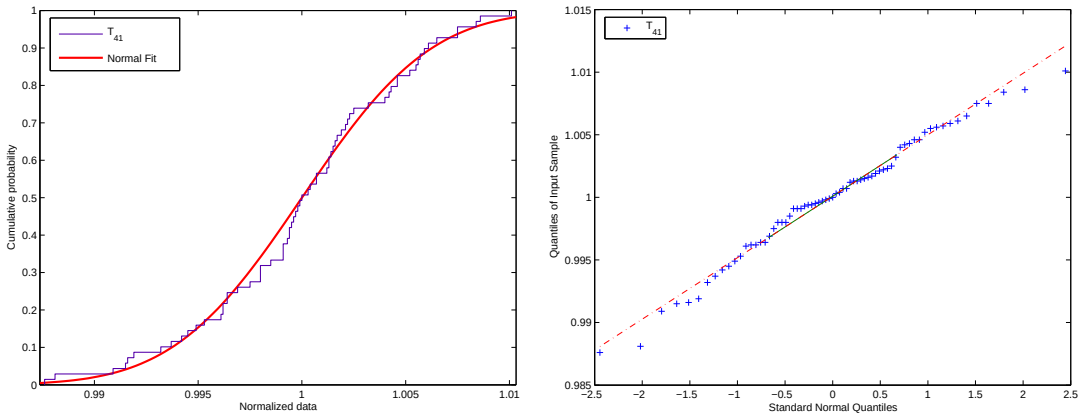

(a) (b)

Figure 2-2: Comparison of T_{41} with ideal normal distribution plotted as (a) cumulative density; (b) quantile-quantile plot.

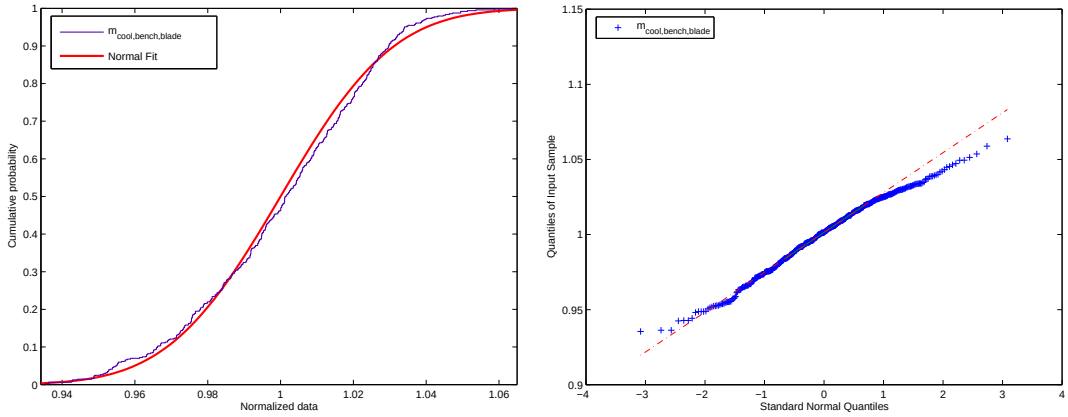

(a) (b)

Figure 2-3: Comparison of $\dot{m}_{cool,bench,blade}$ with ideal normal distribution plotted as (a) cumulative density; (b) quantile-quantile plot.

2.1.4 Correlated Parameters

From the statistical data set for normalized cycle parameters, correlation coefficients indicating relationships between input parameters were computed and are presented in Table 2.3.

Along with the standard deviation of each input parameter, the correlation coefficients are used to create the covariance matrix,

Table 2.3: Correlation coefficients of input parameters.

$\rho_{i,j}$	$T_{3,eng}$	$T_{41,eng}$	$W_{41,eng}$
$T_{3,eng}$	+1	-0.62	+0.54
$T_{41,eng}$	-0.62	+1	-0.55
$W_{41,eng}$	+0.54	-0.55	+1

$$\mathbf{\Sigma} = \begin{bmatrix} \sigma^2_{T_{41,eng}} & \rho_{T_{41,eng},W_{41,eng}}\sigma_{T_{41,eng}}\sigma_{W_{41,eng}} & \rho_{T_{41,eng},T_{3,eng}}\sigma_{T_{41,eng}}\sigma_{T_{3,eng}} \\ \rho_{W_{41,eng},T_{41,eng}}\sigma_{W_{41,eng}}\sigma_{T_{41,eng}} & \sigma^2_{W_{41,eng}} & \rho_{W_{41,eng},T_{3,eng}}\sigma_{W_{41,eng}}\sigma_{T_{3,eng}} \\ \rho_{T_{3,eng},T_{41,eng}}\sigma_{T_{3,eng}}\sigma_{T_{41,eng}} & \rho_{T_{3,eng},W_{41,eng}}\sigma_{T_{3,eng}}\sigma_{W_{41,eng}} & \sigma^2_{T_{3,eng}} \end{bmatrix}. \tag{2.1}$$

To generate the desired correlated variable vector $\mathbf{Y}$ [22] required for Monte Carlo analysis, which will be discussed in Section 3.2, the following transformation is required

$$\mathbf{Y} = \begin{bmatrix} Y_{T_{41,eng}} \\ Y_{W_{41,eng}} \\ Y_{T_{3,eng}} \end{bmatrix} = \mathbf{AX} + \boldsymbol{\mu}, \tag{2.2}$$

where a transformation matrix $\boldsymbol{A}$ is related to the covariance matrix through a Cholesky decomposition

$$\mathbf{\Sigma} = \mathbf{A}\mathbf{A}^T, \tag{2.3}$$

the vector $\mathbf{X}$ is a vector of standard normal variables

$$\mathbf{X} = \begin{bmatrix} N(0,1) \\ N(0,1) \\ N(0,1) \end{bmatrix}, \tag{2.4}$$

and the mean vector is given by

$$\boldsymbol{\mu} = \begin{bmatrix} \mu_{T_{41,eng}} \\ \mu_{W_{41,eng}} \\ \mu_{T_{3,eng}} \end{bmatrix}. \tag{2.5}$$

2.2 One-Dimensional Model

A one-dimensional model of a cooled turbine blade is appropriate for rapid calculations since the problem can be reduced to an algebraic resistance network. It is noted that a single one-dimensional model cannot accurately predict all features simultaneously (e.g. $T_{average,section}$, T_{max}, T_{min}, etc.) but can be constructed to predict one of the variables reasonably well. In this case, the model will be constructed to give a reasonable approximation of $T_{average,section}$.

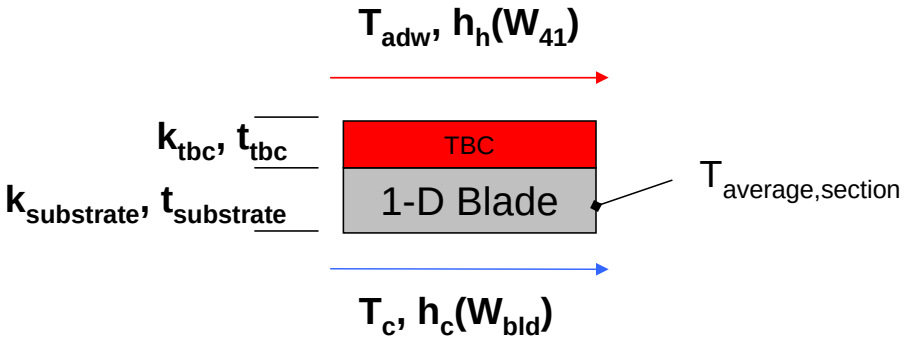

Figure 2-4: One-dimensional model of cooled turbine blade.

The one-dimensional model to be considered is presented in Figure 2-4. The heat transfer rate through the thickness of the model is given by

$$q = \frac{T_{adw} - T_c}{R_{ext,conv} + R_{tbc,cond} + R_{sub,cond} + R_{int,conv}}, \tag{2.6}$$

where thermal resistances are

$$R_{ext,conv} = \frac{1}{h_h\left(W_{41}\right) A_{ext}}, \tag{2.7}$$

$$R_{tbc,cond} = \frac{t_{tbc}}{k_{tbc} A_{ext}}, \tag{2.8}$$

$$R_{sub,cond} = \frac{t_{sub}}{k_{sub}\left(\frac{A_{ext}+A_{int}}{2}\right)}, \tag{2.9}$$

$$R_{int,conv} = \frac{1}{h_c\left(W_{bld}\right) A_{int}}. \tag{2.10}$$

The average section temperature of the substrate can then be calculated from

$$T_{average,section} = T_c + q\left(R_{int,conv} + 0.5R_{sub,cond}\right). \tag{2.11}$$

The input parameters listed in Table 2.1 are used in the following way:

- $T_{41,engine}$ is used to determine the adiabatic wall temperature T_{adw} from

$$T_{adw} = T_{rec} - \eta_{film}\left(T_{rec} - T_{c,exit}\right), where \tag{2.12}$$

$$T_{rec} = T_{41}\frac{1 + \frac{\gamma-1}{2}RM^2}{1 + \frac{\gamma-1}{2}M^2}, and \tag{2.13}$$

$$T_{c,exit} = c_{T_{c,exit}}T_3, \tag{2.14}$$

  with recovery temperature T_{rec}, film effectiveness η_{film}, film exit coolant temperature $T_{c,exit}$, ratio of specific heats γ, recovery factor R, external Mach number M, and scaling factor $(c_{T_{c,exit}})$ between T_3 and $T_{c,exit}$.

- $W_{41,engine}$ is used to scale the external heat transfer coefficient of the form $\mathrm{Re}^{0.8}$, or

$$h_h\left(W_{41}\right) \propto Re^{0.8} = \left(\frac{W_{41,engine}}{W_{41,engine,baseline}}\right)^{0.8} \tag{2.15}$$

- $T_{3,engine}$ is used directly for the coolant side reference temperature (where heat pick-up between compressor discharge and coolant supply is included in the value referred to as $T_{3,engine}$). It is also scaled by $c_{T_{c,exit}}$ to determine the reference film exit coolant temperature.

- $\dot{m}_{cool,blade}$ is used to scale h_c in an equivalent way to $W_{41,engine}$ in Equation 2.15.

- $k_{sub,blade}$ is used in the substrate thermal resistance calculation of Equation 2.9.

- $t_{sub,blade}$ is used in the substrate thermal resistance calculation of Equation 2.9.

- $k_{tbc,blade}$ is used in the tbc thermal resistance calculation of Equation 2.8.

- $t_{tbc,blade}$ is used in the tbc thermal resistance calculation of Equation 2.8.

In order to determine other values required for the model the baseline finite element model is analyzed. Perimeter, area, and volume to surface area ratioing is performed as appropriate to determine all values required.

2.3 Finite Element Model

The high fidelity model used in this research is a finite element model consisting of a preliminary flow network solution, a parametric CAD model which regenerates the geometry needed to mesh the model, and a five section finite element thermal model. For the flow network and finite element thermal models, ANSYS was used. The fidelity of the finite element model is typical of a deterministic model used in industry during preliminary design. A Rolls-Royce provided reference model is based loosely on experience and is thus presented in a normalized fashion.

2.3.1 Flow Network Model

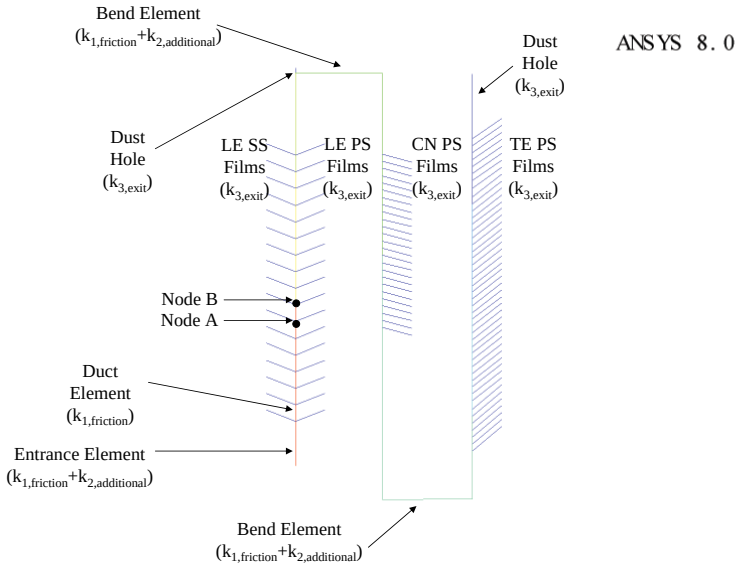

Figure 2-5: Multi-pass flow network model.

For the high fidelity model, the first submodel required is a flow model of the coolant multi-pass network. Unfortunately, a general compressible flow network element type is

not available by default in ANSYS. The flow network model is shown in Figure 2-5. Using incompressible FLUID116 elements [23] along with an average density ρ from the Rolls-Royce model and multiple different types of loss coefficients k, a quasi-compressible model is constructed. Loss coefficients k dictate the velocity in each element by:

$$v = \frac{1}{\sqrt{k}} \frac{2\Delta p}{\rho}. \tag{2.16}$$

The first type of loss which needs to be considered is due to frictional losses in the duct. Using average friction factors provided by Rolls-Royce, the losses in each internal element of the duct can be expressed as:

$$k_{1,friction} = \frac{4 f_{average} l}{D_{hydraulic}}. \tag{2.17}$$

The next loss mechanism to be considered is additional losses due to entrance-effects and duct-bend losses. These losses are assumed to be equal to 1.5 dynamic heads at the entrance, and leading-edge to center and center to trailing-edge bends. The additional losses are added to the friction losses and are expressed as:

$$k_{2,additional} = \frac{1.5 * 2\gamma}{(\gamma - 1) RT_t} \left(1 - \frac{p}{p_t}^{\frac{\gamma-1}{\gamma}} \right). \tag{2.18}$$

The final type of loss to be considered is through the film and dust hole elements. In this case the pressure calculated in the duct represents the total pressure p_t and static exit pressures p at each film location provided by Rolls-Royce will be used on the exterior. The loss coefficient is therefore

$$k_{3,exit} = \frac{2\left(p_t - p\right)\rho}{C_D^2 p_t^2 \frac{2\gamma}{\gamma-1} \frac{p}{p_t}^{\frac{2}{\gamma}} \left[\frac{2\gamma}{(\gamma-1)RT_t} \left(1 - \frac{p}{p_t}^{\frac{\gamma-1}{\gamma}} \right) \right]}. \tag{2.19}$$

The model also needs to take into account the rotating frame of reference of the turbine blade caused by the rotation rate ω. Since reduced pressure $p_{t_{reduced}}$ is constant along a relative streamline, the relative stagnation pressure $p_{t_{rel}}$ between two nodes (i $\rightarrow$ j) in a rotating reference frame can be expressed as:

$$p_{t_{rel_j}} - p_{t_{rel_i}} = \frac{\rho\omega^2}{2} \left[r_j^2 - r_i^2 \right]. \tag{2.20}$$

In the incompressible limit, the static pressure rise p between two nodes r_j and r_i can thus be expressed as:

$$p_{rel_j} - p_{rel_i} = \frac{\rho\omega^2}{2}\left[r_j^2 - r_i^2\right]. \tag{2.21}$$

Thus without any losses, there would be a pressure rise between Nodes A and B of Figure 2-5 which could be calculated from Equation 2.21. Variability enters this model which in turn leads to variability in the finite element thermal model. The input parameters listed in Table 2.2 are used in the following way in this model:

- $D_{SS,LE,blade}$ scales the diameter of the film holes of the suction surface leading edge film row.
- $D_{PS,LE,blade}$, $D_{PS,CN,blade}$, $D_{PS,TE,blade}$ similarly scale the diameters of the corresponding pressure surface film hole rows.

The baseline results as well as perturbations of the model provided by Rolls-Royce were compared with results from the ANSYS solutions for several scenarios which confirmed that the ANSYS quasi-compressible model behaved similarly to the Rolls-Royce compressible model.

2.3.2 CAD/CAPRI Model

In order to facilitate automated regeneration of the geometry, a parametric CAD model is necessary as shown in Figure 2-6. The modeling is designed to capture the nature of the manufacturing process, in that the core is subtracted from the airfoil (corresponding to the removal of the wax core). The individual film cooling holes are replaced with slots so that constant-z sections always give the diameter of the hole. This model created in UniGraphics NX3 allows for modification of most parameters. As a proof-of-concept, only $coreshift_{blade}$ of the model varies, constraining the model such that the number and ordering of faces remains the same for any regeneration. From Table 2.2, coreshift_{blade} shifts the core toward the pressure surface for positive values and toward the suction surface for negative values. In order to ensure robust regeneration, random numbers generated greater than $+4\sigma$ are mapped to $+4\sigma$ and random numbers less than -4σ are mapped to -4σ.

The CAPRI software package [10] allows for hands-off regeneration and also handles the constant-z cuts which form the basis for meshing of the finite element thermal model.

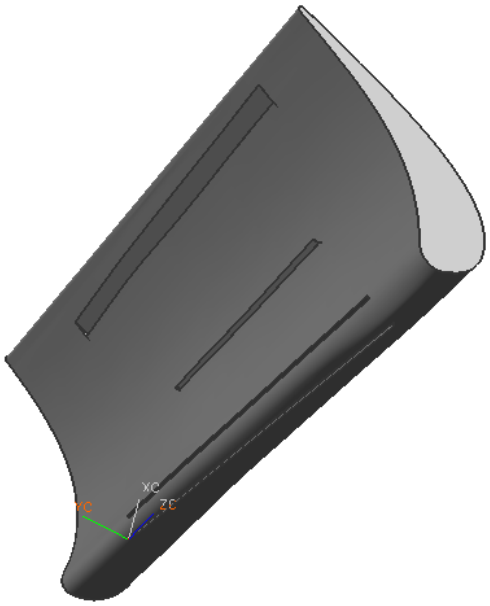

Figure 2-6: UniGraphics NX3 parameterized cooled turbine blade.

2.3.3 Finite Element Thermal Model

Using the constant-z sections provided by CAPRI, a finite element thermal model of the turbine blade can be created as shown in Figure 2-7. Second-order ANSYS PLANE35 elements are used to mesh the sections, which are connected via SURF151 elements with an extra convection node to FLUID116 elements for heat exchange between the cooling flow and the blade. The mass flows calculated from the model of Section 2.3.1 are aggregated and mapped to the nearest element corresponding to the five section model. Exterior heat transfer loads are also modeled using SURF151 elements.

Figure 2-7: Two-dimensional model of cooled turbine blade.

The external flow solution is provided by Rolls-Royce for the baseline model and is assumed to change negligibly for the probabilistic models. The presence of the thermal barrier coating is accounted for by scaling the external heat transfer coefficients provided by the baseline model. The following relation assumes that the heat flux vectors are everywhere normal to the blade surface:

$$h_{tbc} = \frac{h}{1 + Bi}, \tag{2.22}$$

where

$$Bi = \frac{ht_{tbc}}{k_{tbc}}. \tag{2.23}$$

The normalized heat transfer coefficients which are scaled to account for the presence of TBC are shown in Figure 2-8.

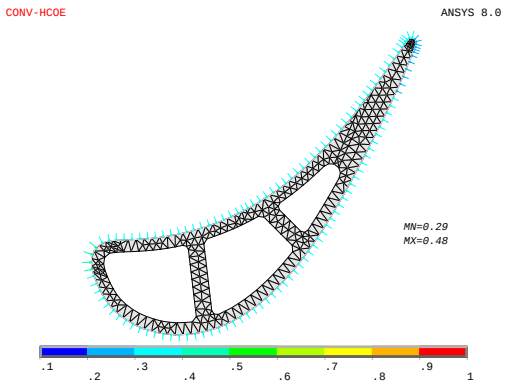

Figure 2-8: Baseline normalized external heat transfer coefficients scaled for presence of TBC.

Similarly, the film hole and internal convection heat transfer is presented in Figures 2-9a and 2-9b, respectively. Note in Figure 2-9b that the heat transfer is enhanced along the side walls of the internal duct, representing the presence of turbulators.

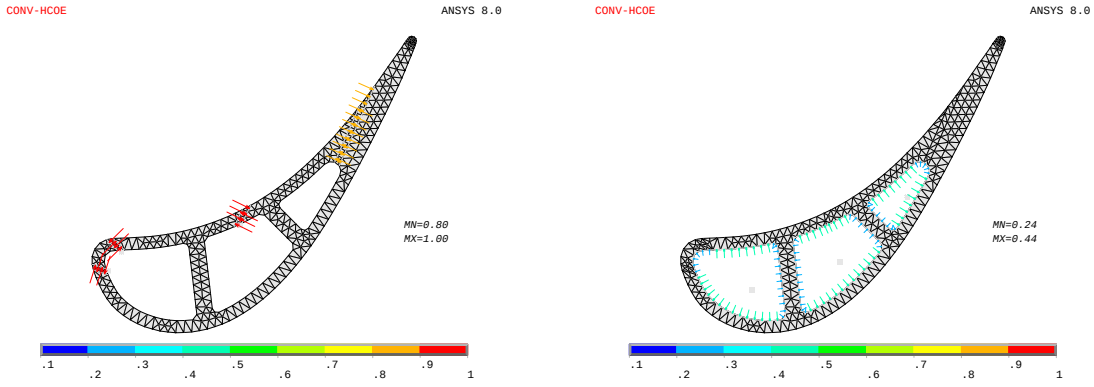

(a) (b)

Figure 2-9: Baseline normalized (a) film cooling hole and (b) internal heat transfer coefficients.

The input parameters of Table 2.2 enter the model in the following ways

- $T_{41,engine}$, $W_{41,engine}$, and $T_{3,engine}$ scale inputs to the model as in the one-dimensional model of Section 2.2.
- $\Delta RTDF_{engine}$ along with $T_{41,engine}$ determines the turbine inlet temperature at each span-wise location as explained in Section 2.1.3.
- $k_{sub,blade}$ is directly entered as a material constant in the finite element thermal model.
- $k_{tbc,blade}$ and $t_{tbc,blade}$ are used to recalculate the scaled external heat transfer coefficient accounting for the presence of TBC as indicated in Equations 2.22 and 2.23.

The baseline solution of the finite element thermal model is presented in Figures 2-10a through 2-10e.

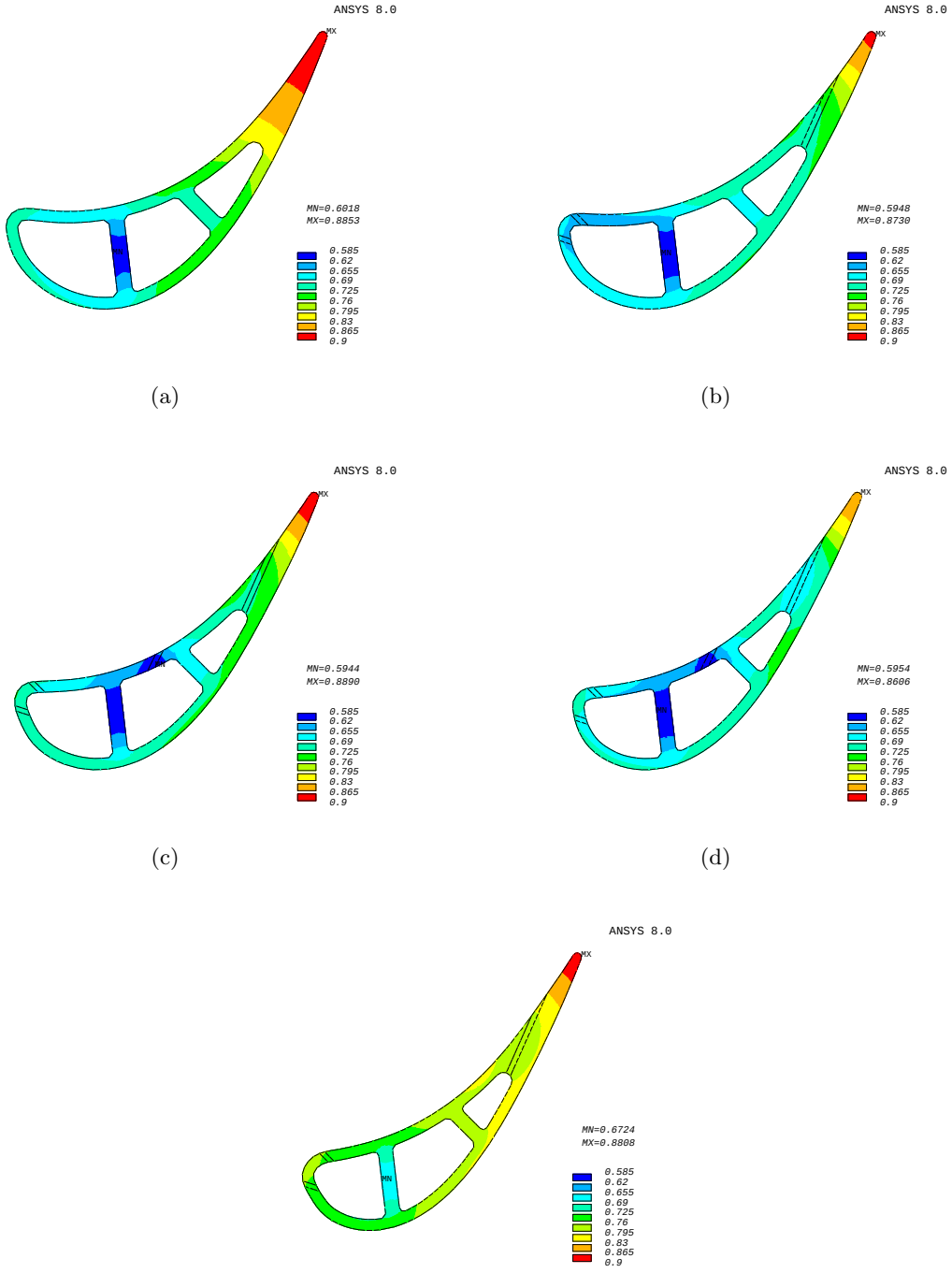

Figure 2-10: Normalized temperature distribution for (a) Section 1 (span=0.10), (b) Section 2 (span=0.31), (c) Section 3 (span=0.52), (d) Section 4 (span=0.74), (e) Section 5 (span=0.90) of baseline model.

Also presented are the solutions for the normalized temperatures of section 3 corresponding to a one-factor-at-a-time shift of the core to $+3\sigma$, -3σ, and the unshifted baseline model in Figures 2-11a through 2-11c.

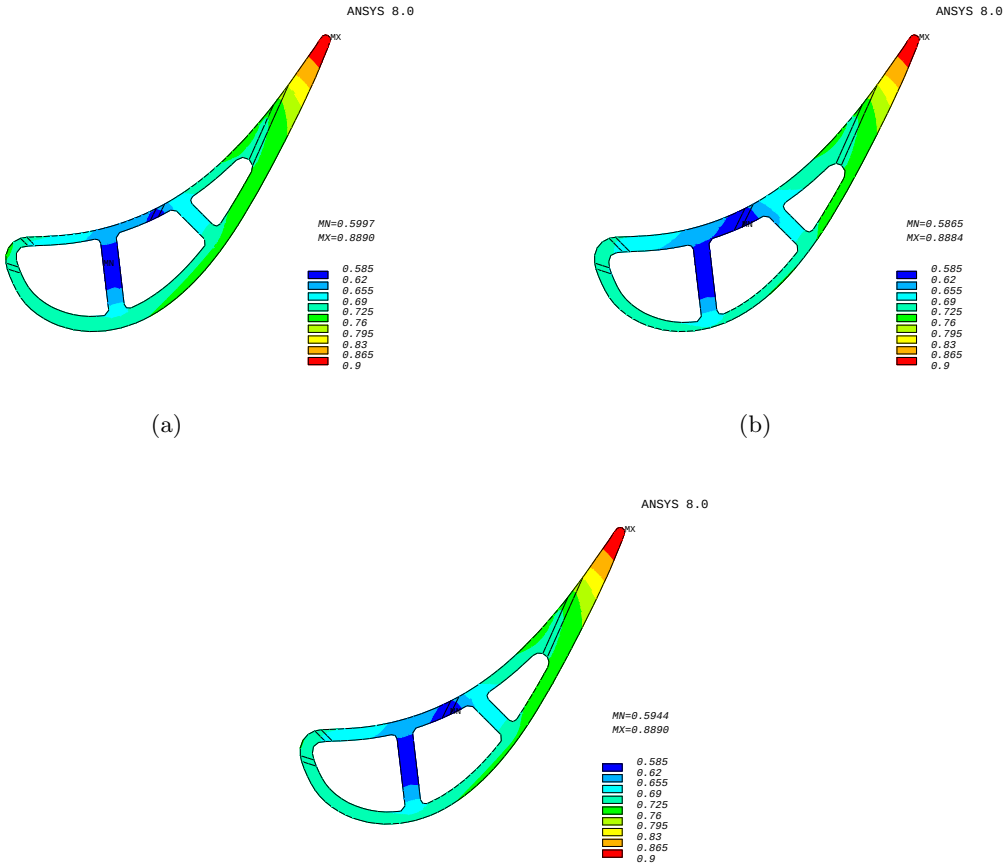

Figure 2-11: Section 3 normalized temperature distribution for (a) coreshift=$+3\sigma$, (b) coreshift=$+3\sigma$, and (c) baseline unshifted model.

2.4 Non-Conformance Indicators

Without a stress model (which would be too computationally expensive) and without proprietary lifing algorithms, the thermal model is used to determine blade non-conformances. Two non-conformance mechanisms are considered: creep and oxidation. The following values will be output from the finite element model (only $T_{average,section}$ output for one-dimensional model):

- Creep indicator, section 2 $T_{average,section}$, is chosen to investigate creep life. $T_{average,section}$ is the quantity which is traditionally used to investigate creep of a critical section. Section 2 is the most radially inward section (all radially outward sections apply centrifugal load driving creep) with film cooling.

- Oxidation indicator 1, section 3 T_{max} is used as one output to investigate oxidation life. In the baseline model T_{max} is at the trailing edge tip of section 3.

- Oxidation indicator 2, section 3 $T_{average,PS}$ is used as the second output to investigate life. It is generally accepted that oxidation at the trailing edge tip is to be expected, since trailing edge tip temperatures tend toward the external adiabatic wall temperature. The indicator $T_{average,PS}$ is a measure of possible oxidation non-conformances in a more critical area, e.g. mid chord, where aerodynamic performance could be diminished by oxidation, requiring even higher T_{41} to maintain thrust. Section 3 is chosen because it has the hotter $T_{average,PS}$ of the two sections (3 and 4) featuring film cooling at the leading edge, center, and trailing edge.

2.5 Tolerancing Schemes

The current state of manufacturing of a first stage turbine blade is such that most tolerances involved are minimized under the constraint that the parts be economically feasible to produce. Non-conformances in the field could likely be avoided by substantially reducing the acceptable manufacturing tolerances, but would likely necessitate a more expensive manufacturing technique to yield a satisfactory number of parts. However, by utilizing more stringent tolerances and thus rejecting a small number of additional parts, costly in-service non-conformances can be avoided with minimal impact to part yield. This research will deal with not including units from the tail of each input parameter's distribution, the so called "bad-range", which causes the engine to be more likely to exhibit a non-conformance. In practice, the implementation of this scheme involves not building blades from the bad-range of a blade-to-blade level parameter and/or not shipping an engine exhibiting a parameter from the bad-range of an engine-to-engine level parameter at pass-off test. Engines found to have a non-conforming engine-to-engine level parameter could be reworked to address the non-conformance before being returned to the pass-off test.

2.6 Cost Structure

For the purpose of evaluating cost ramifications related to blade robustness a simple cost structure model was employed:

- The cost of a non-conformance in the field is assumed to have a cost of A.
- The cost of manufacturing each blade is B.
- The cost of rejecting an engine for rework as a result of a failed pass-off test at the manufacturer is C.

A tolerancing scheme can be characterized by $\alpha_{salvage}$, the number of non-conformances salvaged from a fleet which would have $\alpha_{baseline}$ non-conformances if nothing is done, β blades that are manufactured but never used due to a blade-to-blade level parameter being in the bad-range, and γ engines that need to be reworked due to an engine-to-engine parameter being in the bad-range. For a fleet subject to a tolerancing scheme, the relevant costs are

- the avoided cost of non-conformances in the field is $\alpha_{salvage}$A,
- the cost of the "bad-range" blades manufactured but not used is βB,
- the cost of engines requiring rework is γC.

While the true value of each of these costs is proprietary, characteristic ratios of the costs can be used. These non-dimensional cost ratios (B/A, C/A) are varied to demonstrate that even under wildly different cost assumptions, the recommended tolerancing schemes are still money-making initiatives. By normalizing the costs involved by the cost of the field non-conformances which would occur if nothing is done, $\alpha_{baseline}$A, a net normalized profit π can be calculated from

$$\pi = \frac{\alpha_{salvage}}{\alpha_{baseline}} - \frac{(\beta B + \gamma C)}{\alpha_{baseline} A}. \tag{2.24}$$

If π is greater than zero, the tolerancing-scheme is a money-making initiative. A maximum theoretical value of π=1 implies that all engines which would have been non-conforming were salvaged by a tolerancing scheme which cost nothing to implement. It should be noted, that a money-losing initiative is not limited to π=-1. To calculate the net-profit in units of currency, π is simply multiplied by $\alpha_{baseline}$A.

Chapter 3

Probabilistic Techniques

A key component of any engineering analysis is determining what level of fidelity is appropriate. To that end, both a one-dimensional and a finite element model were presented in Chapter 2. However, probabilistic analysis requires solving multiple instances of a model. Thus, the choice of model fidelity coupled with the choice of the probabilistic technique determines how much time will be required for the solution. The probabilistic techniques pursued in this research include one-factor-at-a-time response surface, fractional-factorial response surface, and Monte Carlo analysis. Only the results for the creep indicator of the finite element model will be presented in this chapter for conciseness. The effect of inputs simultaneously varying at the blade-to-blade and engine-to-engine levels requires non-conformances to be classified in such a way that all input parameters can be ranked and compared. A scheme for classifying non-conformances in an equivalent manner for both blade-to-blade and engine-to-engine parameters will be introduced in Section 3.2.4.

3.1 Response Surface

Response surface methodology is a technique traditionally applied to investigating and/or optimizing processes through the use of designed experiments. The response surface analysis process is typically sequential, such that a relatively large list of input parameters are initially investigated through a screening experiment. The screening experiment is used to determine if some input parameters can be dropped from subsequent analysis where a higher-order response surface is constructed. For the screening experiment, a one-factor-at-a-time linear response surface will be constructed; which will eventually lead into a quadratic

fractional-factorial response surface [24, 25].

3.1.1 One-Factor-at-a-Time Linear Response Surface

A one-factor-at-a-time linear response surface is the simplest response surface that can be constructed, and is analogous to a traditional sensitivity analysis. The coefficients of a one-factor-at-a-time linear response surface can be interpreted as the linear effect of perturbing each input parameter separately. To determine the response surface of an output variable, a design must be chosen which perturbs the input parameters in such a way as to minimize the error of the response surface relative to the original model. For consistency with the fractional-factorial quadratic response surface presented in the next section, the input parameters will be perturbed to both $\pm 1\sigma$; although a one-sided perturbation is appropriate if run-time needs to be minimized.

A factor-setting matrix D is constructed with each column corresponding to coded-variable settings of either 0 or ± 1 for each of the input variables. A coded variable of 0 corresponds to μ the mean value and ± 1 corresponds to $\mu \pm \sigma$. The dimensions of D are thus 25×12 for the finite element model corresponding to the settings of the 12 input variables for each of the 25 runs necessary to capture the behavior of the baseline model and two perturbations for each input. A design matrix X (25×13) is then constructed from D corresponding to 1 constant term, and 12 linear terms.

The response surface equation [24] can then be written as

$$y = X\beta + \epsilon, \tag{3.1}$$

where β is an unknown vector of the regression coefficients and ϵ is a vector of random errors. A least squares technique is used to minimize

$$L = \sum_{i=1}^{n} \epsilon_i^2 = \epsilon'\epsilon = (y - X\beta)'(y - X\beta). \tag{3.2}$$

Expanding L, equation 3.2 can be expressed as

$$L = y'y - 2\beta' X'y + \beta' X' X\beta. \tag{3.3}$$

The vector of least squares estimators b is the vector such that

$$\frac{\partial L}{\partial \beta}|_b = -2X'y + 2X'Xb = 0. \tag{3.4}$$

Solving for Equation 3.4, b the least squares estimator of β is

$$b = \left(X'X\right)^{-1} X'y. \tag{3.5}$$

The response surface regression model is thus an estimate given by

$$\hat{y} = Xb, \tag{3.6}$$

with residual vector e given by

$$e = y - \hat{y}. \tag{3.7}$$

The one-factor-at-a-time linear terms of the response surface for creep indicator, section 2 $T_{average,section}$, of the finite element model are presented in Table 3.1. Also presented are the linear terms of the response surface for creep indicator of the one-dimensional model. These effects will be ranked and compared with rankings determined from non-conformance classifications in Chapters 4.

Table 3.1: Creep indicator response terms, section 2 $T_{average,section}$ (screening FE), $T_{average,section}$ (screening 1D).

Linear Terms:

	FE β_i **(K)**	**1D** β_i **(K)**
$T_{41,eng}$	+3.669	+3.329
$\Delta RTDF_{eng}$	+0.399	N/A
$W_{41,eng}$	+0.242	+0.223
$T_{3,eng}$	+1.054	+1.326
$D_{SS,LE,bld}$	-0.563	N/A
$D_{PS,LE,bld}$	-0.608	N/A
$D_{PS,CN,bld}$	-0.316	N/A
$D_{PS,TE,bld}$	-5.940	N/A
$\dot{m}_{cool,bld}$	N/A	-3.478
$k_{sub,bld}$	+0.139	-0.035
$coreshift_{bld}$	+1.891	N/A
$t_{sub,bld}$	N/A	0.035
$k_{tbc,bld}$	+1.411	+1.382
$t_{tbc,bld}$	-2.820	-2.763

3.1.2 Fractional-Factorial Quadratic Response Surface

Factorial designs allow for interactions between input parameters to be investigated in addition to the linear effects of each parameter. However, with k input parameters, the required 2^k simulations is usually too computationally expensive. If the experimenter can assume that high-order interaction terms are negligible, low-order interactions can be obtained with significantly fewer simulations through a fractional-factorial design [24].

MATLAB 7.0 includes a fractional-factorial design generator, ccdesign, as part of the Statistics Toolbox. The design generator is limited to 11 factors, which is one more than the number of input parameters considered in this problem. It will be shown in Section 3.2.4 that engine-to-engine level parameters are expected to be weaker than blade-to-blade level parameters, so interaction terms involving the weakest cycle parameter $W_{41,eng}$ will not be included. By initially omitting $W_{41,eng}$, a face-centered, quarter-fraction, central composite design of 531 runs can be constructed using the MATLAB ccdesign function. All variable perturbations are chosen to be of magnitude 1σ, a compromise between capturing the linearity of the inputs near the center of the normal distribution and accurately predicting the response in the tails of the distribution. A design matrix X (531x78) is then constructed from D corresponding to 1 constant term, 11 linear terms, 11 second-order variable-squared terms and 55 second-order interaction terms. By now including the $\pm 1\sigma$ runs for $W_{41,eng}$ from the one-factor-at-a-time analysis, the design matrix X can be augmented to (533x79), which will now include the linear effect of $W_{41,eng}$. A regression is then performed following the procedure of the previous section. The fractional-factorial quadratic response surface for the creep indicator, section 2 $T_{average,section}$, is presented in Table 3.2, normalized by $T_{41,eng,baseline}$.

Table 3.2: Creep indicator response terms, section 2 $T_{average,section}$ (RS FEM).

Linear Terms:

	β_i **(K)**
$T_{41,eng}$	+3.670
$\Delta RTDF_{eng}$	+0.400
$W_{41,eng}$	+0.242
$T_{3,eng}$	+1.054
$D_{SS,LE,bld}$	-0.564
$D_{PS,LE,bld}$	-0.610
$D_{PS,CN,bld}$	-0.313
$D_{PS,TE,bld}$	-5.937
$k_{sub,bld}$	+0.139
$coreshift_{bld}$	+1.891
$k_{tbc,bld}$	+1.409
$t_{tbc,bld}$	-2.820

Second Order Terms:

$\beta_{i,j}$ **(K)**	$T_{41,eng}$	$\Delta RTDF_{eng}$	$T_{3,eng}$	$D_{SS,LE,bld}$	$D_{PS,LE,bld}$	$D_{PS,CN,bld}$	$D_{PS,TE,bld}$	$k_{sub,bld}$	$coreshift_{bld}$	$k_{tbc,bld}$	$t_{tbc,bld}$
$T_{41,eng}$	-3.41e-04	-1.17e-05	-1.64e-04	-4.68e-03	-5.05e-03	-2.59e-03	-4.80e-02	+1.13e-03	+1.60e-02	+1.14e-02	-2.29e-02
$\Delta RTDF_{eng}$	-	-3.41e-04	-1.17e-05	-3.63e-04	-4.26e-04	-3.24e-04	-6.24e-03	-1.17e-05	+3.09e-03	+1.48e-03	-2.94e-03
$T_{3,eng}$	-	-	+1.59e-04	+1.22e-03	+1.30e-03	+7.42e-04	+1.16e-02	-2.89e-04	-4.25e-03	-2.78e-03	+5.58e-03
$D_{SS,LE,bld}$	-	-	-	+1.16e-03	+1.49e-02	+1.42e-02	+2.16e-02	-2.05e-03	+1.07e-02	-4.49e-04	+8.40e-04
$D_{PS,LE,bld}$	-	-	-	-	+2.16e-03	+1.47e-02	+2.26e-02	-2.58e-03	+3.30e-02	-5.51e-04	+1.06e-03
$D_{PS,CN,bld}$	-	-	-	-	-	+1.17e-02	+4.75e-02	-6.95e-04	+1.44e-03	-3.91e-06	+3.91e-06
$D_{PS,TE,bld}$	-	-	-	-	-	-	+2.24e-01	-8.27e-03	-2.55e-02	+2.49e-03	-4.99e-03
$k_{sub,bld}$	-	-	-	-	-	-	-	-3.34e-03	-3.58e-03	+2.95e-03	-5.94e-03
$coreshift_{bld}$	-	-	-	-	-	-	-	-	-2.43e-02	+5.47e-04	-1.05e-03
$k_{tbc,bld}$	-	-	-	-	-	-	-	-	-	-4.23e-02	+7.48e-02
$t_{tbc,bld}$	-	-	-	-	-	-	-	-	-	-	+1.92e-02

3.2 Monte Carlo

While the response surfaces created in the previous sections are appropriate for determining effects and interactions, further analysis is required to determine how the blade-to-blade and engine-to-engine level parameters combine probabilistically to affect the operation of a single engine. In this section, a Monte Carlo method is presented in which a fleet of engines is constructed and explicitly modeled using the statistical data and assumptions on the input parameters discussed in Chapter 2.

3.2.1 Monte Carlo of Response Surfaces

Response surfaces are amenable to efficient simulations of an entire fleet of engines. Solution time is trivial for the algebraic calculations required, such that even large fleets of engines can be constructed. For consistency and comparison, the same random numbers are used for the one-factor-at-a-time Monte Carlo, the fractional-factorial Monte Carlo and the finite element Monte Carlo. A fleet size of 500 engines consisting of 70 blades per engine is used as the basis for this analysis.

3.2.2 Monte Carlo of Finite Element Model

Another, more conservative approach, is to use the finite element model to explicitly model each of the 70 blades per engine in all of the 500 engines in the fleet. The computational expense of this model is approximately one month of run-time for a single CPU. In practice, a cluster of computers could be used to reduce run-time by grouping smaller batches for several of the time-intensive steps of the process. A flow chart of the process is included in Figure 3-1 to show all of the steps required. Note: MATLAB, CAPRI, and ANSYS scripts as well as a fully-parametric CAD model were developed to automate this process.

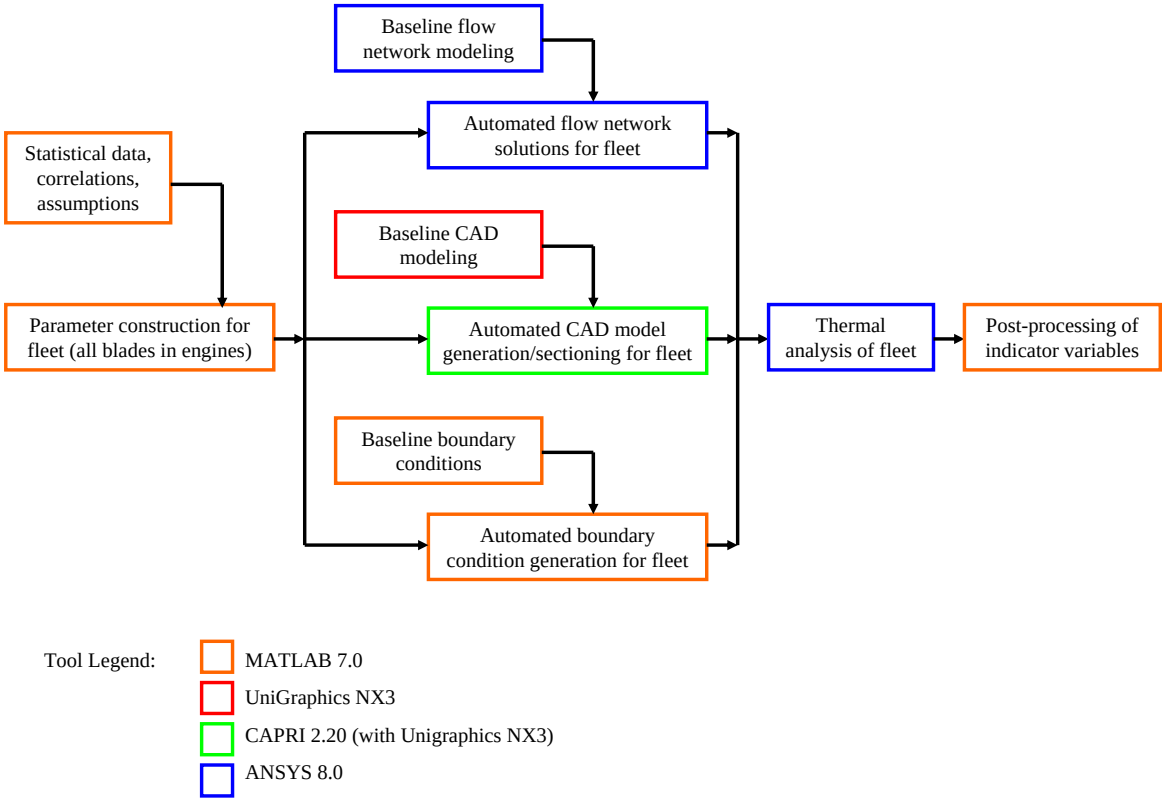

Figure 3-1: Flow chart showing process for fleet analysis.

3.2.3 Comparison of Response Surface Models to Finite Element Models

Using the same random numbers, the errors of both the one-factor-at-a-time and the fractional-factorial response surfaces relative to the finite element solutions, ($T_{average,section,RS}$-$T_{average,section,FE}$), were computed for the 35,000 blade Monte Carlo simulation. Histograms of the error of both response-surfaces are plotted in Figure 3-2. It is noted in Table 3.3 that slight non-linearities cause the one-factor-at-a-time solution to have a slightly negative mean value of the error, $\mu(error)$=-0.172 K. The second-order terms of the fractional-factorial response surface significantly improve upon the approximation to the finite element results, such that the standard deviation of the error is only $\sigma(error)$=0.039 K. The excellent a posteriori agreement between the Monte Carlo simulations on the fractional-factorial response surface and the explicit finite element runs indicate that, for this heat transfer problem, the fractional-factorial response surface likely yields sufficient resolution.

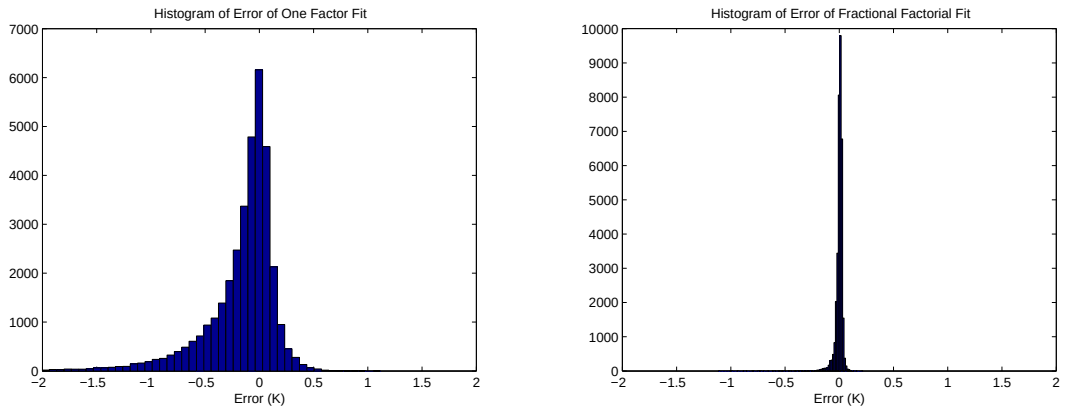

(a) (b)

Figure 3-2: Histogram of error of (a) one-factor-at-a-time; (b) fractional-factorial response surfaces relative to finite element creep indicator solutions.

Table 3.3: Statistics of error of response surfaces relative to finite element creep indicator solutions.

type of response surface	$\mu(error)$	$\sigma(error)$
one-factor-at-a-time	-0.172	0.360
fractional-factorial	-0.001	0.039

3.2.4 Quantifying Parameter Effects

A common, deterministic approach is to rank the sensitivity of an output parameter (e.g. $T_{average,section}$) to a change in each input. This is easily done by ranking the magnitude of the coefficients of a response-surface. For example, according to Table 3.2, the most sensitive parameter would be $D_{PS,TE,bld}$, followed by $T_{41,eng}$ and $t_{tbc,bld}$. This view, however, ignores the fact that an engine consists of multiple blades (e.g. 70 first-stage turbine blades in the hypothetical engine considered in this thesis) and therefore a large deviation in a blade parameter is much more likely to be present in an engine than a large deviation in an engine parameter [2, 15]. More succinctly, for each engine, a blade-to-blade level parameter has 70 chances to have a larger variation while and an engine-to-engine level parameter has only one chance. Table 3.4 shows quantitatively the difference in probability for engine-to-engine and blade-to-blade level parameters (assuming 70 blades per engine) occurring at least once per engine in a one-sided 1, 2, and 3σ normal-distribution tail. For example, a $\geq+3\sigma$ variation in an engine parameter has a probability of only 0.001, while a $\geq+3\sigma$ variation in at least one blade in an engine has a probability of 0.09, nearly 100 times larger. Thus, quantifying the importance of each parameter's variability must appropriately account for the likelihood of the parameter occurring.

Table 3.4: Probability of input parameter occurring in bad-range at least once in an engine containing 70 first-stage turbine blades.

Bad-Range Tail Cutoff	$Prob_{eng-to-eng}$	$Prob_{bld-to-bld}$
$> 1\sigma$	0.159	1.000
$> 2\sigma$	0.023	0.800
$> 3\sigma$	0.001	0.090

The quantification method proposed here is based on classifying engine non-conformances. Engine non-conformance is assumed to occur when a non-conformance indicator (as described in Section 2.4) is outside an acceptable range for at least one blade. For example, if one blade of an engine has an average section temperature which is larger than some pre-determined threshold, the engine is non-conforming. The classification of engine non-conformances begins by assigning each input parameter a bad-range as described in Section 2.5. Checking for a non-conformance as a result of an engine-to-engine level parameter being in the bad-range is trivial. However, for blade-to-blade level parameters, each of which occurs 70 times in an engine, a more complex classification scheme is required. The broad-

est class is labeled "correlation" and a non-conforming engine is in this class for a specific blade-to-blade level input parameter if it has at least one blade with this input parameter in a bad range. This correlation class is then broken into three more restrictive classes:

- Conclusive: All non-conforming blades in engine have blade-level parameter in bad-range.
- Contributing: Engine has more than one non-conforming blade, but not all non-conforming blades have blade-level parameter in bad-range.
- Coincidence: Engine is non-conforming but none of the non-conforming blades have blade-level parameter in bad-range.

In the remainder of this thesis, conclusive non-conformances are used to rank the relative importance of both blade-to-blade and engine-to-engine level input parameters. Note that engine-to-engine level parameters are always conclusive when the engine is non-conforming and the engine level parameter is in its bad range.

3.2.5 Augmentation of Finite Element Model Runs

Chapter 5 will include explicit modeling of tolerancing schemes, with the motivation that some manufactured blades could be omitted from an engine, and some engines could be reworked after a pass-off test before being shipped to a customer. Therefore, it is necessary to develop a method to quantify the impact of these tolerancing schemes. The simplest way to model this would be to actually run each possible scenario, rejecting the units from the random-number generator which do not fit into the current tolerancing scheme being investigated. However, this approach will limit the number of tolerancing schemes considered, since the computational time for a fleet of finite element models requires approximately one month (on one CPU).

An alternative, is to augment the finite element model run matrix such that there are sufficient engines in excess with excess blades in each engine so that the desired fleet size could still be constructed from an augmented run matrix. In order to be able to simultaneously tolerance (at the 1σ single-sided level) one input parameter at the engine-to-engine level along with two input-parameters at the blade-to-blade level, an augmented run matrix was found to conservatively require 605 engines with 105 blades per engine. Thus

an additional 28,525 simulations must be performed. It should be noted that, numerically, the engines cannot actually be reworked (as in practice) in the sense that the blades are used again after a cycle parameter is found out-of tolerance during a pass-off test. However, there is no statistical reason why the next engine's blades will be any different than the previous rejected engine's blades since the cycle parameters are independent of the blade parameters in this model. By using an augmented run matrix, the possibilities which can be investigated using a tolerance scheme are essentially unlimited, and do not require more than a rearranging of the post-processed quantities to form a fleet matrix of 500 engines with 70 blades per engine.

Chapter 4

Analysis of Variability

By applying the probabilistic techniques presented in the previous section, the effect of engine non-conformances with respect to the input parameters of the problem can be investigated. It was suggested in Section 3.2.4 that a linear sensitivity analysis is insufficient when input parameters are varying at multiple levels. This chapter highlights the importance of this effect.

4.1 Linear Sensitivity

The one-factor-at-a-time linear response terms for creep indicator of both the finite element model and the one-dimensional resistance network model are presented in Table 4.1. The terms presented in Table 3.1 are normalized by the magnitude of the strongest effect ($\beta_{D_{PS,TE,bld}}$ =-5.940 K) and then Pareto-ranked. It should be noted that in the finite element cooling-flow network, $D_{PS,TE,bld}$ acts as the strongest "meter" of the blade, essentially setting the overall blade cooling mass flow. For the one-dimensional model, there are no separate film rows, and the cooling flow of the blade is determined only by one parameter, $\dot{m}_{cool,bld}$. For comparison purposes using the same random numbers, $\dot{m}_{cool,bld}$ is used from the output of the computationally-inexpensive initial flow network solution. It is noted that

- there is strong trend-wise agreement between the finite element model and the one-dimensional model for all terms except the conduction-related parameters of the substrate, which have a relatively weak effect anyway;
- the parameters which either meter or directly determine the overall cooling mass flow,

$D_{PS,TE,bld}$ for the finite element model and $\dot{m}_{cool,bld}$ for the one-dimensional model, have the strongest linear effect;

- the linear effect of the next strongest term, $T_{41,eng}$, is almost as strong as that of the cooling mass flow terms.

Table 4.1: Normalized and Pareto-ranked creep indicator response terms, section 2 $T_{average,section}$ (screening FE), $T_{average,section}$ (screening 1D).

Linear Terms:

	FE $\beta_{i,normalized}$	**1D** $\beta_{i,normalized}$
$D_{PS,TE,bld}$	-1.000	N/A
$\dot{m}_{cool,bld}$	N/A	-0.586
$T_{41,eng}$	+0.618	+0.560
$t_{tbc,bld}$	-0.475	-0.465
$coreshift_{bld}$	+0.318	N/A
$k_{tbc,bld}$	+0.238	+0.233
$T_{3,eng}$	+0.177	+0.223
$D_{PS,LE,bld}$	-0.102	N/A
$D_{SS,LE,bld}$	-0.095	N/A
$\Delta RTDF_{eng}$	+0.057	N/A
$D_{PS,CN,bld}$	-0.053	N/A
$W_{41,eng}$	+0.041	+0.038
$k_{sub,bld}$	+0.023	-0.006
$t_{sub,bld}$	N/A	0.006

The discrepancy of the linear effect of the one-dimensional substrate conduction parameters relative to the finite element substrate conduction parameters highlights the shortcomings of the one-dimensional model. The parameter coreshift$_{bld}$ is replaced with a single wall thickness, $t_{sub,bld}$, which does not accurately account for changes in $T_{average,section}$ of the higher-fidelity model. Similarly, there is weak agreement between the effect of $k_{sub,bld}$ for the two models. This is because $k_{sub,bld}$ is directly related to conduction, which is a complex two-dimensional phenomenon in the finite element model as opposed to simple one-dimensional conduction. In both models, conduction through the thermal barrier coating is assumed to be one dimensional. As expected by this consistent assumption, the agreement of the linear sensitivities of $t_{tbc,bld}$ and $k_{tbc,bld}$ is quite good between the two models.

4.2 Conclusive Engine Non-Conformances Results

To compare the engine-to-engine and blade-to-blade level parameters directly, the number of conclusive engine non-conformances occurring for the subset of engines which have an input parameter in the bad-range are presented in Table 4.2. The non-conformance temperature is defined to be at the B_{90} level, meaning that 10 percent of the engines will contain at least one blade with a temperature higher than the non-conformance temperature. There are thus 50 engines from the 500 engine baseline fleet which are non-conforming, which is the theoretical maximum of any entry in Table 4.2.

At this point, it is appropriate to compare the values in Table 4.2 between engine-to-engine and blade-to-blade level parameters. These values represent the maximum theoretical number of engines which could be salvaged by a tolerancing scheme which would replace the input parameters in the bad-range. In Table 4.2, and in subsequent tables, tolerancing ranges which have a potential to salvage more than 20 engines (40% of the non-conforming engines in the fleet) are highlighted in yellow.

The parameter with the largest number of conclusive engine non-conformances given the parameter is in the bad range is $D_{PS,TE,bld}$ which exhibited 48 conclusive engine non-conformances at the 1σ level and 44 conclusive engine non-conformances at the 2σ level. Note that the strongest engine-to-engine level parameter was $T_{41,eng}$ with 22 conclusive engine non-conformances at the 1σ level and 3 conclusive engine non-conformances at the 2σ level. At the 1σ level, $T_{41,eng}$ only exhibits 0.46 of the conclusive engine non-conformances that $D_{PS,TE,bld}$ does. At the 2σ level, this ratio is only 0.07. Both of these values are smaller than the 0.618 ratio of the linear sensitivities between the two parameters presented in Table 4.1. Also, note that the input parameter $t_{tbc,bld}$ exhibits 27 conclusive engine non-conformances at the 1σ level, which is more than the 22 conclusive engine non-conformances from $T_{41,eng}$. That is to say, the order of the Pareto-ranking of these parameters is different than the linear sensitivity ranking suggests as presented in Table 4.1. The expected effect of an increased importance of blade-to-blade level parameters (relative to what might be incorrectly concluded from a linear sensitivity analysis) is confirmed.

Table 4.2: Number of conclusive engine non-conformances for creep indicator.

Finite Element Simulations

Cycle Parameters					Flow Network Parameters						Conduction Parameters				
Range	# (Conclusive) Engine NC Given BR				Range	# Conclusive Engine NC Given BR					Range	# Conclusive Engine NC Given BR			
	$T_{41,eng}$	$\Delta RTDF_{eng}$	$W_{41,eng}$	$T_{3,eng}$		$D_{SS,LE,bld}$	$D_{PS,LE,bld}$	$D_{PS,CN,bld}$	$D_{PS,TE,bld}$	$m_{cool,bld}$		$k_{sub,bld}$	$cr\text{-}shft_{,bld}$	$k_{tbc,bld}$	$t_{tbc,bld}$
>1σ	22	10	8	12	>1σ	15	7	9	48	44	>1σ	7	14	18	27
>2σ	3	0	0	2	>2σ	4	1	1	44	26	>2σ	0	4	3	7
>3σ	0	0	0	1	>3σ	1	1	0	16	10	>3σ	0	1	0	2

Fractional-Factorial Response Surface

Range	# (Conclusive) Engine NC Given BR				Range	# Conclusive Engine NC Given BR					Range	# Conclusive Engine NC Given BR			
	$T_{41,eng}$	$\Delta RTDF_{eng}$	$W_{41,eng}$	$T_{3,eng}$		$D_{SS,LE,bld}$	$D_{PS,LE,bld}$	$D_{PS,CN,bld}$	$D_{PS,TE,bld}$	$m_{cool,bld}$		$k_{sub,bld}$	$cr\text{-}shft_{,bld}$	$k_{tbc,bld}$	$t_{tbc,bld}$
>1σ	22	10	8	12	>1σ	15	7	9	49	N/A	>1σ	7	14	18	27
>2σ	3	0	0	2	>2σ	4	1	1	45	N/A	>2σ	0	4	3	7
>3σ	0	0	0	1	>3σ	1	1	0	16	N/A	>3σ	0	1	0	2

One-Factor-at-a-Time Response Surface

Range	# (Conclusive) Engine NC Given BR				Range	# Conclusive Engine NC Given BR					Range	# Conclusive Engine NC Given BR			
	$T_{41,eng}$	$\Delta RTDF_{eng}$	$W_{41,eng}$	$T_{3,eng}$		$D_{SS,LE,bld}$	$D_{PS,LE,bld}$	$D_{PS,CN,bld}$	$D_{PS,TE,bld}$	$m_{cool,bld}$		$k_{sub,bld}$	$cr\text{-}shft_{,bld}$	$k_{tbc,bld}$	$t_{tbc,bld}$
>1σ	24	8	10	13	>1σ	14	6	7	48	N/A	>1σ	6	14	22	28
>2σ	4	0	0	3	>2σ	4	2	0	40	N/A	>2σ	0	5	4	8
>3σ	0	0	0	1	>3σ	1	1	0	10	N/A	>3σ	0	2	1	3

One-Dimensional Model

Range	# (Conclusive) Engine NC Given BR				Range	# Conclusive Engine NC Given BR					Range	# Conclusive Engine NC Given BR			
	$T_{41,eng}$	$\Delta RTDF_{eng}$	$W_{41,eng}$	$T_{3,eng}$		$D_{SS,LE,bld}$	$D_{PS,LE,bld}$	$D_{PS,CN,bld}$	$D_{PS,TE,bld}$	$m_{cool,bld}$		$k_{sub,bld}$	$t_{sub,bld}$	$k_{tbc,bld}$	$t_{tbc,bld}$
>1σ	29	N/A	11	12	>1σ	N/A	N/A	N/A	N/A	49	>1σ	12	7	26	37
>2σ	4	N/A	0	1	>2σ	N/A	N/A	N/A	N/A	22	>2σ	2	1	7	16
>3σ	0	N/A	0	1	>3σ	N/A	N/A	N/A	N/A	11	>3σ	0	0	1	4

Another important trend is the relative strength of $\dot{m}_{cool,bld}$ compared to $D_{PS,TE,bld}$. At the 1σ level, the ratio of conclusive engine non-conformances is 0.92 when comparing the 44 conclusive engine non-conformances of $\dot{m}_{cool,bld}$ to the 48 conclusive engine non-conformances of $D_{PS,TE,bld}$. However, by the 2σ level, this ratio has reduced to 0.59 (26:44). This implies that even though the aggregate cooling flow through the blade, $\dot{m}_{cool,bld}$, is a strong parameter, the diameter of the film cooling hole at the trailing edge, $D_{PS,TE,bld}$, is an even stronger parameter. This is because not only does $D_{PS,TE,bld}$ tend to act as the meter of the blade, but it also affects the heat transfer in a critical location, the trailing edge tip.

Table 4.2 also contains the results for the fractional-factorial response surfaces, the one-factor-at-a-time response surface, and the one-dimensional model. What is important is that with the exception of some slight discrepancies related to the parameter $D_{PS,TE,bld}$, the fractional-factorial response surface matches the predictions of the finite element solution. Excellent agreement is to be expected because of the small error of the fractional-factorial response surface shown in Figure 3-2b. However, since $\dot{m}_{cool,bld}$, is an intermediate output variable of the finite element flow-network model, the fractional-factorial response surface does not yield important information regarding the comparison of $\dot{m}_{cool,bld}$ to $D_{PS,TE,bld}$. Also note that there is excellent trend-wise agreement between the finite element simulations and the one-factor-at-a-time response surface and the one-dimensional model. It should again be noted that these lower-fidelity models cannot predict the effects of all of the input parameters explicitly modeled in the finite element model.

4.3 Confidence Range Analysis

One important question which needs to be answered is whether the conclusions drawn from the 500 engine sample are statistically significant. Probability theory offers a means to answer this question. Specifically, an estimate $\hat{P}$ of the probability P of conclusive engine non-conformances from an input parameter in the bad-range is given by:

$$\hat{P}\left(\text{non-conformance}_{\text{engine,conclusive}}\text{for an input}\right) = \frac{\text{number of conclusive engine NC for an input}}{\text{number of engines}}. \tag{4.1}$$

For a (1-α) confidence interval, the range of the probability P can be expressed as a function of the sample probability [26]:

$$\hat{P} - Z_{\frac{\alpha}{2}}\sqrt{\frac{\left(\hat{P}\right)\left(1-\hat{P}\right)}{\text{number of engines}}} < P < \hat{P} + Z_{\frac{\alpha}{2}}\sqrt{\frac{\left(\hat{P}\right)\left(1-\hat{P}\right)}{\text{number of engines}}}, \tag{4.2}$$

where $Z_{\frac{\alpha}{2}}$ is the area under the $\frac{\alpha}{2}$ tail of the normal curve.

The range of the probability estimated by the sample probability is presented in Table 4.3 to 0.90 confidence. The ranges presented indicate some overlap amongst the ranges of interest which are highlighted. However, the 500 engine fleet size is determined to be marginally sufficient for parameter-ranking purposes as a result of the following conclusions:

- $D_{PS,TE,bld}$ at 1σ and 2σ is statistically better than $T_{41,eng}$ at 1σ.
- $t_{tbc,bld}$ at 1σ is not statistically better than $T_{41,eng}$ at 1σ.
- $D_{PS,TE,bld}$ is better than $t_{tbc,bld}$ when comparing the same σ-level.

Table 4.3: Probability (0.90 confidence) of conclusive engine non-conformance from an input for creep indicator of finite element simulations.

Cycle Parameters

Range	P(non-conformance$_{engine,(conclusive)}$ for an input)			
	$T_{41,eng}$	$\Delta RTDF_{eng}$	$W_{41,eng}$	$T_{3,eng}$
>1σ	0.044±0.015	0.020±0.010	0.016±0.009	0.024±0.011
>2σ	0.006±0.006	0.000±0.000	0.000±0.000	0.004±0.005
>3σ	0.000±0.000	0.000±0.000	0.000±0.000	0.002±0.003

Flow Network Parameters

Range	P(non-conformance$_{engine,(conclusive)}$ for an input)				
	$D_{SS,LE,bld}$	$D_{PS,LE,bld}$	$D_{PS,CN,bld}$	$D_{PS,TE,bld}$	$m_{cool,bld}$
>1σ	0.030±0.013	0.014±0.009	0.018±0.010	0.096±0.022	0.088±0 .021
>2σ	0.008±0.007	0.002±0.003	0.002±0.003	0.088±0.021	0.052±0 .016
>3σ	0.002±0.003	0.002±0.003	0.000±0.000	0.032±0.013	0.020±0 .010

Conduction Parameters

Range	P(non-conformance$_{engine,(conclusive)}$ for an input)			
	$k_{sub,bld}$	cr-shft$_{,bld}$	$k_{tbc,bld}$	$t_{tbc,bld}$
>1σ	0.014±0.009	0.028±0.012	0.036±0.014	0.054±0.017
>2σ	0.000±0.000	0.008±0.007	0.006±0.006	0.014±0.009
>3σ	0.000±0.000	0.002±0.003	0.000±0.000	0.004±0.005

Chapter 5

Tolerance Assessment

The analysis of variability in the Section 4.2 is limited to providing the maximum theoretical number of engines which could be salvaged if a tolerancing scheme were implemented. In addition to addressing input parameters which would cause non-conformances in the field, any tolerancing scheme will likely replace some units which would not have exhibited a non-conformance in the field. One noteworthy example is that in a one-factor blade-to-blade tolerancing scheme there is a possibility for bad-range blades which would not have non-conformed in a specific engine to be replaced by blades which do non-conform in that engine, likely as a result of a different parameter being in its bad-range. By augmenting the Monte Carlo simulations (Section 3.2.5) to allow for an investigation of tolerancing schemes; an efficient cost-benefit analysis of tolerancing alternatives can be performed.

5.1 Salvaged Engine Non-Conformances

The B_{90} non-conformance criteria given in Chapter 4 implies that the baseline design is expected to have 10% of the engines in the fleet non-conform, or 50 non-conforming engines for the 500 engine fleet. For a tolerancing sheme, the number of salvaged engines is the number of engines less than the expected number of 50 engine non-conformances. By post-processing the creep indicator of the finite element augmented Monte Carlo simulations, the number of engines salvaged by various tolerancing schemes is calculated and presented in Tables 5.1 and 5.2.

Table 5.1: Number of salvaged engine non-conformances for creep indicator of single-factor tolerancing.

Finite Element Simulations

	Cycle Parameters				Flow Network Parameters					Conduction Parameters			
Tolerance	# of Salvaged Engines				# of Salvaged Engines					# of Salvaged Engines			
	$T_{41,eng}$	$\Delta RTDF_{eng}$	$W_{41,eng}$	$T_{3,eng}$	$D_{SS,LE,bld}$	$D_{PS,LE,bld}$	$D_{PS,CN,bld}$	$D_{PS,TE,bld}$	$m_{cool,bld}$	$k_{sub,bld}$	$cr\text{-}shft_{bld}$	$k_{tbc,bld}$	$t_{tbc,bld}$
>1σ	22	5	7	11	9	4	6	48	44	0	9	15	21
>2σ	3	0	-1	1	3	-1	-1	44	26	-3	3	2	4
>3σ	0	0	0	1	1	1	-1	16	10	0	1	0	1

Fractional-Factorial Response Surface

	Cycle Parameters				Flow Network Parameters					Conduction Parameters			
Tolerance	# of Salvaged Engines				# of Salvaged Engines					# of Salvaged Engines			
	$T_{41,eng}$	$\Delta RTDF_{eng}$	$W_{41,eng}$	$T_{3,eng}$	$D_{SS,LE,bld}$	$D_{PS,LE,bld}$	$D_{PS,CN,bld}$	$D_{PS,TE,bld}$	$m_{cool,bld}$	$k_{sub,bld}$	$cr\text{-}shft_{bld}$	$k_{tbc,bld}$	$t_{tbc,bld}$
>1σ	22	5	7	11	9	4	6	49	N/A	0	9	15	21
>2σ	3	0	-1	1	3	-1	-1	45	N/A	-3	3	2	4
>3σ	0	0	0	1	1	1	-1	16	N/A	0	1	0	1

One-Factor-at-a-Time Response Surface

	Cycle Parameters				Flow Network Parameters					Conduction Parameters			
Tolerance	# of Salvaged Engines				# of Salvaged Engines					# of Salvaged Engines			
	$T_{41,eng}$	$\Delta RTDF_{eng}$	$W_{41,eng}$	$T_{3,eng}$	$D_{SS,LE,bld}$	$D_{PS,LE,bld}$	$D_{PS,CN,bld}$	$D_{PS,TE,bld}$	$m_{cool,bld}$	$k_{sub,bld}$	$cr\text{-}shft_{bld}$	$k_{tbc,bld}$	$t_{tbc,bld}$
>1σ	23	2	7	10	8	2	4	48	N/A	1	9	20	23
>2σ	4	0	-1	2	3	1	-2	39	N/A	-2	4	3	6
>3σ	0	0	0	1	1	1	0	10	N/A	0	2	1	3

One-Dimensional Model

	Cycle Parameters				Flow Network Parameters					Conduction Parameters			
Tolerance	# of Salvaged Engines				# of Salvaged Engines					# of Salvaged Engines			
	$T_{41,eng}$	$\Delta RTDF_{eng}$	$W_{41,eng}$	$T_{3,eng}$	$D_{SS,LE,bld}$	$D_{PS,LE,bld}$	$D_{PS,CN,bld}$	$D_{PS,TE,bld}$	$m_{cool,bld}$	$k_{sub,bld}$	$t_{sub,bld}$	$k_{tbc,bld}$	$t_{tbc,bld}$
>1σ	28	N/A	8	8	N/A	N/A	N/A	N/A	49	4	-1	23	32
>2σ	4	N/A	-1	0	N/A	N/A	N/A	N/A	22	0	0	6	13
>3σ	0	N/A	0	1	N/A	N/A	N/A	N/A	11	0	0	1	4

Table 5.2: Number of salvaged engine non-conformances for creep indicator of two-factor tolerancing of finite element simulations.

	# of Salvaged Engines		
Tolerance	$D_{PS,TE,bld}$>1σ	$D_{PS,TE,bld}$>2σ	$D_{PS,TE,bld}$>3σ
$T_{41,eng}$>1σ	50	49	33
$T_{41,eng}$>2σ	49	47	19
$T_{41,eng}$>3σ	48	44	16

Table 5.1 represents a single-factor tolerancing scheme, where separate fleets are constructed while tolerancing one parameter at a time. In practice, this could be implemented by rejecting the bad-range blades before they are ever built into the engines. Comparisons are included between the lower fidelity models and the finite element model. As predicted in Section 4.2, the cooling flow parameters, $D_{PS,TE,bld}$ and $\dot{m}_{cool,bld}$ are the most effective blade-to-blade level parameters to tolerance. For example, rejecting $D_{PS,TE,bld}$ at the 2σ level salvaged 44 engines, while a marginal improvement of 48 salvaged engines is realized at the 1σ level. Another blade-to-blade parameter of interest is $\dot{m}_{cool,bld}$, which salvaged 26 engines at the 2σ level, while realizing a substantial improvement to 44 engines at the 1σ level. Also, it should be noted that while overall cooling flow variability, $\dot{m}_{cool,bld}$, is important, further data of flow variability through the metering passage at the trailing edge can lead to even more effective tolerancing. If these results were found for an actual engine, it would be recommended that every blade be flow-checked and that the check include masking techniques.

Tolerancing schemes on both $D_{PS,TE,bld}$ and $\dot{m}_{cool,bld}$ were more effective than the best engine-to-engine level parameter to tolerance, $T_{41,eng}$, which salvaged 22 engines when toleranced at the 1σ level. In contrast with the results of Table 4.2, at the 1σ level, $t_{tbc,bld}$ is slightly less effective than $T_{41,eng}$ with 21 salvaged engines compared to 22. In agreement with Table 4.2, the fractional-factorial response surface shows minimal discrepancies with the finite element model results, with only a few negligible line item differences for the parameter $D_{PS,TE,bld}$. The lower fidelity one-factor-at-a-time response surface and one-dimensional models show similar trend-wise agreement with the finite element model for the parameters which the lower fidelity models are able to predict.

Tolerancing schemes need not be limited to single-factor tolerancing. In practice, a two-factor scheme could be implemented by first rejecting bad-range blades from being built into an engine and then reworking the engines which exhibit a bad-range engine-to-engine level parameter which would become apparent during a pass-off test before the engine is shipped to a customer. Numerically, the augmented engine framework does not allow for the blades from an engine with a bad-range engine-to-engine level parameter to be reused, whereas in practice the blades could be reused. However, there is no statistical risk to this discrepancy, since the blades are not modeled to affect the engine-to-engine level parameters, and there is no statistical preference of the blades between engines.

Table 5.2 investigates a fleet constructed in such a way that not only rejects the bad-range of the strongest blade-to-blade level parameter, $D_{PS,TE,bld}$, but also doesn't ship engines in which strongest engine-to-engine level parameter, $T_{41,eng}$, is in the bad range. It is evident, that there is a compounding effect due to the interaction of ensuring that no engine contains either of these parameters in their respective bad-ranges. Simultaneously tolerancing $D_{PS,TE,bld}$ and $T_{41,eng}$ both at the 2σ level salvages 47 of the 50 expected non-conforming engines and is highlighted as a recommended tolerancing scheme for profitability reasons which will be presented in the Section 5.2.

Another figure of merit for a tolerancing scheme is what percentage of conclusive engine non-conformances from the baseline simulation were salvaged by the scheme. Numerically, this is the ratio of the salvaged engines (entries of Table 5.1) to the maximum theoretical number of salvaged engines (entries of Table 4.2). Figure 5-1 plots this ratio relative to number of conclusive engine non-conformances from the baseline simulation for tolerancing schemes with greater than 5 possible engines which can be salvaged. It is clear that schemes which address more conclusive-engine non-conformances from the baseline simulation have a higher ratio of success at actually salvaging the engines. Also, it is noted that there are no clear trends differentiating schemes at the engine-to-engine and blade-to-blade level, confirming that the metrics being used to analyze the inputs are on an equal level.

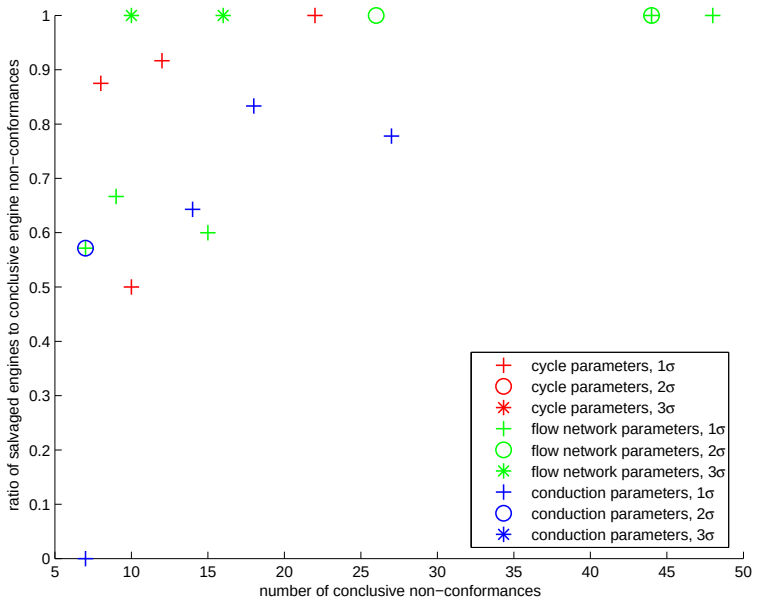

Figure 5-1: Ratio of salvaged engines to conclusive engine non-conformances for creep indicator of finite element simulations.

5.2 Profitability Analysis

The profitability of a tolerancing scheme was first discussed in Section 2.6. To determine if a tolerancing scheme is a money-making initiative, the costs associated would need to be known. These figures are proprietary, but by assuming that the ratios of the costs are

$$\frac{cost\,of\,blade}{cost\,of\,engine\,non-conformance\,in\,field} = \frac{B}{A} = 0.001,$$
$$\frac{cost\,to\,rework\,engine}{cost\,of\,engine\,non-conformance\,in\,field} = \frac{C}{A} = 0.1,$$

the normalized profitabilities of the tolerancing schemes can be calculated using the simple cost model described in Section 2.6. These normalized profitabilities are presented in Tables 5.3 and 5.4.

Table 5.3: Normalized profitability of single-factor tolerancing for creep indicator of finite element simulations.

Cycle Parameters

Tolerance	Normalized Profitability, π			
	$T_{41,eng}$	$\Delta RTDF_{eng}$	$W_{41,eng}$	$T_{3,eng}$
>1σ	0.276	-0.106	-0.044	0.042
>2σ	0.048	-0.020	-0.044	-0.008
>3σ	0.000	0.000	-0.002	0.018

Flow Network Parameters

Tolerance	Normalized Profitability, π				
	$D_{SS,LE,bld}$	$D_{PS,LE,bld}$	$D_{PS,CN,bld}$	$D_{PS,TE,bld}$	$m_{cool,bld}$
>1σ	0.047	-0.052	-0.015	0.829	0.749
>2σ	0.044	-0.035	-0.037	0.864	0.504
>3σ	0.019	0.019	-0.021	0.319	0.199

Conduction Parameters

Tolerance	Normalized Profitability, π			
	$k_{sub,bld}$	cr-shft$_{,bld}$	$k_{tbc,bld}$	$t_{tbc,bld}$
>1σ	-0.131	0.044	0.165	0.288
>2σ	-0.076	0.044	0.023	0.064
>3σ	-0.001	0.019	-0.001	0.019

Table 5.4: Normalized profitability of two-factor tolerancing for creep indicator of finite element simulations.

Normalized Profitability, π			
Tolerance	$D_{PS,TE,bld}$>1σ	$D_{PS,TE,bld}$>2σ	$D_{PS,TE,bld}$>3σ
$T_{41,eng}$>1σ	0.706	0.800	0.495
$T_{41,eng}$>2σ	0.837	0.912	0.367
$T_{41,eng}$>3σ	0.829	0.864	0.319

What Table 5.3 indicates is that (subject to the assumptions of the non-conformance criteria, modeling, and cost structure) between π=0.276 and π=0.864 of the cost associated with non-conformances in the field can be saved through the highlighted single-factor tolerancing schemes. The best single-factor tolerancing scheme is $D_{PS,TE,bld}$, which at the 2σ level recovers π=0.864 of the cost associated with non-conformances occurring in the field. The trend of specific knowledge about $D_{PS,TE,bld}$, instead of gross knowledge of $\dot{m}_{cool,bld}$, allows for a larger normalized profit (only π=0.504 for the 2σ level tolerancing of $\dot{m}_{cool,bld}$). Both of these schemes are significantly better than π=0.276 attainable by tolerancing $T_{41,eng}$ at the 1σ level, or π=0.288 from tolerancing $t_{tbc,bld}$ at the 1σ level. The best option, seen in Table 5.4, is to tolerance both $D_{PS,TE,bld}$ and $T_{41,eng}$ at the 2σ level simultaneously, which can lead to π=0.912 relative to the cost associated with non-conformances in the field.

The ratios of the costs involved in this analysis are difficult to approximate. Therefore, it would be prudent to determine if the tolerancing schemes would be profitable under substantially different cost structures. Figure 5-2 presents a contour plot of a normalized profit solution space for tolerancing both $D_{PS,TE,bld}$ and $T_{41,eng}$ at the 1σ level simultaneously. The center of this plot represents the assumed cost structure indicated above, with both the x-axis (B/A) and the y-axis (C/A) extending logarithmically one order of magnitude in both directions from the center. The contour plot includes a gray-scale representing profit from (0 to +1) and an equivalent red-scale representing net loss from (0 to -1). It is noted that the net losses can extend beyond -1. Figure 5-2 shows how the normalized profit is affected for various cost structures, and has its characteristic shape because of the two-factor tolerancing. Note, that from the center of Figure 5-2, as C/A increases, the cost of rework becomes larger relative to the cost of a non-conformance in the field. Eventually, the cost of rework becomes so expensive that the tolerancing scheme becomes a money-losing initiative and the contour turns red. Similarly, as B/A increases, the cost of manufacturing each blade relative to the cost of a non-conformance in the field becomes larger. Eventually, this change in cost structure would indicate that the toleracing scheme would be a money-losing initiative. However, the logarithmic nature of Figure 5-2, indicates that at the center of the figure, the scheme is a stable money-making initiative of π=0.706. Figure 5-3 presents all options for this two-factor tolerancing space. Note that the profitability of the recommended scheme, where both $D_{PS,TE,bld}$ and $T_{41,eng}$ are simultaneously toleranced at the 2σ level is extremely stable to drastic changes in cost structure.

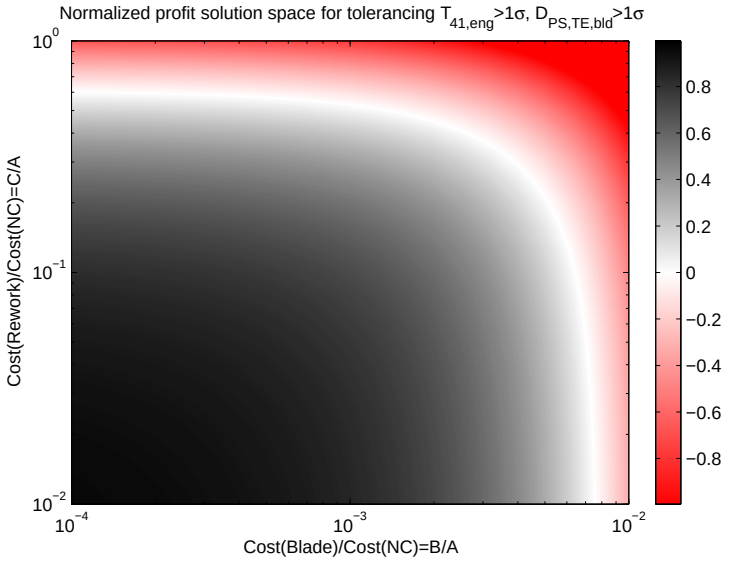

Figure 5-2: Normalized profit solution space for two-factor tolerancing $T_{41,engine} > 1\sigma$, $D_{PS,TE,bld} > 1\sigma$.

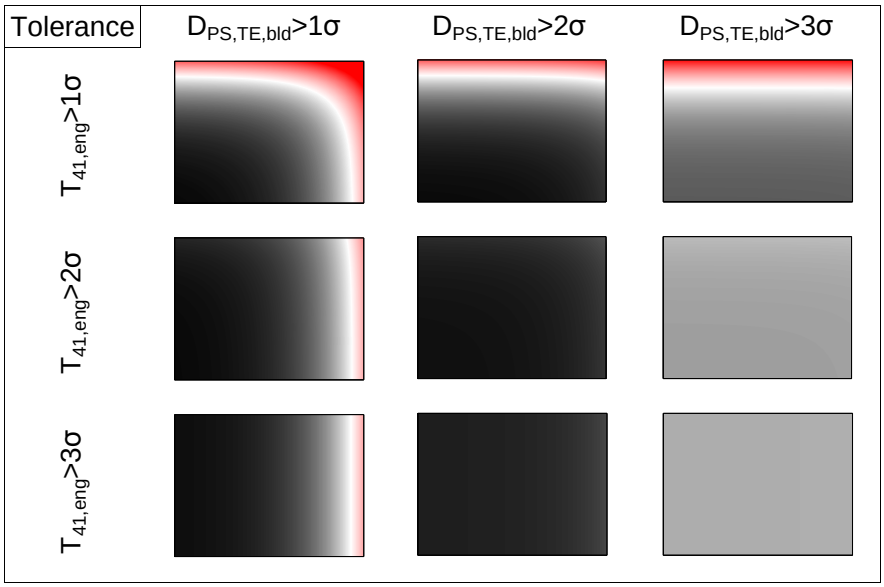

Figure 5-3: Normalized profit solution space for various two-factor tolerancing schemes of $T_{41,engine}$ and $D_{PS,TE,bld}$.

Chapter 6

Summary and Conclusions

This work served to demonstrate that modern computing resources and software allows for automated analysis which can enable probabilistic simulations on a large scale. Specifically applied to a first-stage turbine blade, it was demonstrated that:

- A parameterized finite element thermal model can be constructed which allows for robust simulation of multiple instances.
- Monte Carlo techniques can allow for an analysis of input parameters that occur at multiple levels to be analyzed simultaneously, and tolerancing schemes of the input parameters ranked accordingly. This exposes a key weakness of linear-sensitivity analyses when input parameters occur at different levels.
- Monte Carlo techniques indicate that a two-factor simultaneous tolerancing scheme of $D_{PS,TE,bld}$ and $T_{41,eng}$ is the most promising for reducing creep-induced non-conformances.
- Response surface and one-dimensional models can be used to approximate the trend-wise behavior of a finite element thermal model for a fleet of engines.

It is thus recommended that if the assumptions involved in this research are consistent with the experience on an engine program, a flow-check of every cooled-turbine blade assembled into an engine is appropriate. Further benefits can be realized by combining knowledge of total cooling flow through the blade with masking some exits to determine flow through critical areas.

Toward the end goal of recommending which analysis yields the best return-on-investment relative to computational costs, it is advised that the various techniques pursued be further

challenged as the problem is extended and re-posed. With the extension of this work to proprietary non-linear lifing trends, it is possible that the excellent agreement between the finite element model, response surfaces, and one-dimensional models seen in this research will break down.

It is also noted that recent advances in parametric CAD-model construction, coupled with the CAPRI software package to handle automated regeneration of the model, opens up many doors for probabilistic analyses investigating manufacturing variability. While this work demonstrated that regeneration and subsequent sectioning and meshing of a model can be robust for a single CAD parameter varying (coreshift$_{bld}$), there are numerous scenarios which could be considered to challenge and further develop the technology. Some examples would include how to handle automated meshing when feature birth and death occurs and when inconsistent face-numbering results from parameter variability.

Another possible area of future work related to turbine blades would be to use the techniques developed in this work to combine a thermal analysis with a stress/lifing analysis. This type of analysis would introduce strong physics-based non-linearities which the current problem does not include.

Appendix A

Oxidation Indicator 1 Summary

A.1 One-Factor-at-a-Time Response Surface

Table A.1: Oxidation indicator 1 response terms, section 3 T_{max} (screening FEM).

Linear Terms:

	β_i (K)
$T_{41,eng}$	+5.484
$\Delta RTDF_{eng}$	+2.151
$W_{41,eng}$	+0.149
$T_{3,eng}$	+0.735
$D_{SS,LE,bld}$	+0.005
$D_{PS,LE,bld}$	+0.004
$D_{PS,CN,bld}$	-0.014
$D_{PS,TE,bld}$	-2.243
$k_{sub,bld}$	-2.284
$coreshift_{bld}$	+0.066
$k_{tbc,bld}$	+0.770
$t_{tbc,bld}$	-1.538

A.2 Fractional-Factorial Response Surface

Table A.2: Oxidation indicator 1 response terms, section 3 T_{max} (RS FEM).

Linear Terms:

	β_i **(K)**
$T_{41,eng}$	+5.484
$\Delta RTDF_{eng}$	+2.151
$W_{41,eng}$	+0.149
$T_{3,eng}$	+0.735
$D_{SS,LE,bld}$	+0.004
$D_{PS,LE,bld}$	+0.004
$D_{PS,CN,bld}$	-0.014
$D_{PS,TE,bld}$	-2.243
$k_{sub,bld}$	-2.283
$coreshift_{bld}$	+0.067
$k_{tbc,bld}$	+0.770
$t_{tbc,bld}$	-1.538

Second Order Terms:

$\beta_{i,j}$ **(K)**	$T_{41,eng}$	$\Delta RTDF_{eng}$	$T_{3,eng}$	$D_{SS,LE,bld}$	$D_{PS,LE,bld}$	$D_{PS,CN,bld}$	$D_{PS,TE,bld}$	$k_{sub,bld}$	$coreshift_{bld}$	$k_{tbc,bld}$	$t_{tbc,bld}$
$T_{41,eng}$	-3.80e-04	+4.24e-04	-1.82e-04	+1.95e-06	-2.54e-05	-1.31e-04	-1.62e-02	-1.62e-02	+5.53e-04	+5.27e-03	-1.04e-02
$\Delta RTDF_{eng}$	-	+1.20e-04	+2.54e-05	+7.62e-05	+8.79e-05	+4.49e-05	-7.18e-03	-8.51e-03	+8.01e-05	+2.62e-03	-5.20e-03
$T_{3,eng}$	-	-	+6.20e-04	+2.54e-05	+1.37e-05	+4.10e-05	+3.55e-03	+3.27e-03	-1.43e-04	-1.01e-03	+1.89e-03
$D_{SS,LE,bld}$	-	-	-	+6.20e-04	+7.99e-04	+9.67e-04	+4.67e-04	+2.05e-04	+4.10e-05	-9.77e-06	+3.71e-05
$D_{PS,LE,bld}$	-	-	-	-	+1.12e-03	+1.00e-03	+4.63e-04	+1.62e-04	+5.53e-04	-1.37e-05	+4.10e-05
$D_{PS,CN,bld}$	-	-	-	-	-	+2.62e-03	+3.65e-03	-7.25e-04	+8.93e-04	+2.25e-04	-4.16e-04
$D_{PS,TE,bld}$	-	-	-	-	-	-	+5.31e-02	-6.65e-02	-7.25e-04	+1.96e-02	-3.96e-02
$k_{sub,bld}$	-	-	-	-	-	-	-	+2.56e-02	+4.53e-03	+1.65e-02	-3.33e-02
$coreshift_{bld}$	-	-	-	-	-	-	-	-	-1.38e-03	-8.34e-04	+1.68e-03
$k_{tbc,bld}$	-	-	-	-	-	-	-	-	-	-2.69e-02	+5.47e-02
$t_{tbc,bld}$	-	-	-	-	-	-	-	-	-	-	-3.38e-03

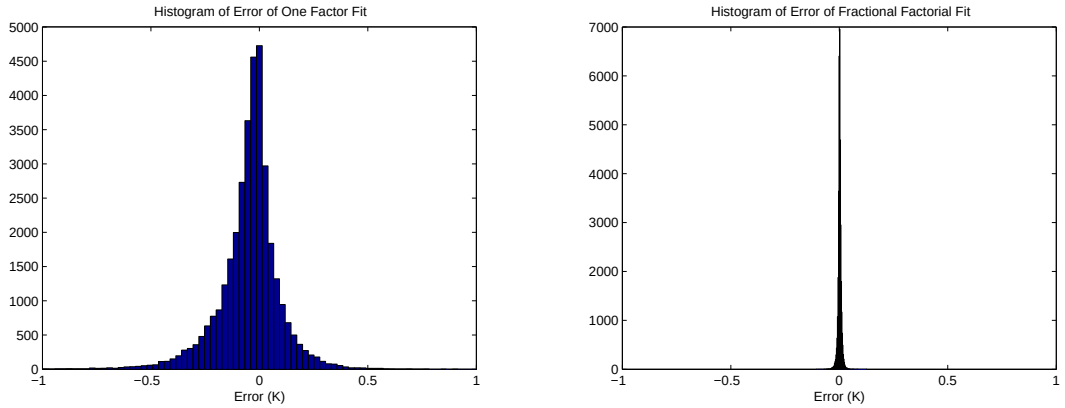

(a) (b)

Figure A-1: Histogram of error of (a) one-factor-at-a-time; (b) fractional-factorial response surfaces relative to finite element oxidation indicator 1 solutions.

Table A.3: Statistics of error of response surfaces relative to finite element oxidation indicator 1 solutions.

type of response surface	$\mu(error)$	$\sigma(error)$
one-factor-at-a-time	-0.046	0.144
fractional-factorial	0.002	0.008

A.3 Monte Carlo Simulations

Table A.4: Number of conclusive engine non-conformances for oxidation indicator 1.

Finite Element Simulations

Range	# (Conclusive) Engine NC Given BR			
	$T_{41,eng}$	$\Delta RTDF_{eng}$	$W_{41,eng}$	$T_{3,eng}$
>1σ	36	22	19	20
>2σ	6	3	3	4
>3σ	0	0	0	1

Range	# Conclusive Engine NC Given BR				
	$D_{SS,LE,bld}$	$D_{PS,LE,bld}$	$D_{PS,CN,bld}$	$D_{PS,TE,bld}$	$m_{cool,bld}$
>1σ	3	2	4	23	14
>2σ	0	0	1	7	2
>3σ	0	0	0	1	1

Range	# Conclusive Engine NC Given BR			
	$k_{sub,bld}$	cr-shft$_{bld}$	$k_{tbc,bld}$	$t_{tbc,bld}$
>1σ	21	2	6	15
>2σ	8	1	1	2
>3σ	3	0	0	0

Fractional-Factorial Response Surface

Range	# (Conclusive) Engine NC Given BR			
	$T_{41,eng}$	$\Delta RTDF_{eng}$	$W_{41,eng}$	$T_{3,eng}$
>1σ	36	22	19	20
>2σ	6	3	3	4
>3σ	0	0	0	1

Range	# Conclusive Engine NC Given BR				
	$D_{SS,LE,bld}$	$D_{PS,LE,bld}$	$D_{PS,CN,bld}$	$D_{PS,TE,bld}$	$m_{cool,bld}$
>1σ	3	2	4	23	N/A
>2σ	0	0	1	7	N/A
>3σ	0	0	0	1	N/A

Range	# Conclusive Engine NC Given BR			
	$k_{sub,bld}$	cr-shft$_{bld}$	$k_{tbc,bld}$	$t_{tbc,bld}$
>1σ	21	2	6	15
>2σ	8	1	1	2
>3σ	3	0	0	0

One-Factor-at-a-Time Response Surface

Range	# (Conclusive) Engine NC Given BR			
	$T_{41,eng}$	$\Delta RTDF_{eng}$	$W_{41,eng}$	$T_{3,eng}$
>1σ	35	22	19	19
>2σ	6	3	3	4
>3σ	0	0	0	1

Range	# Conclusive Engine NC Given BR				
	$D_{SS,LE,bld}$	$D_{PS,LE,bld}$	$D_{PS,CN,bld}$	$D_{PS,TE,bld}$	$m_{cool,bld}$
>1σ	3	3	5	23	N/A
>2σ	0	1	1	7	N/A
>3σ	0	0	0	1	N/A

Range	# Conclusive Engine NC Given BR			
	$k_{sub,bld}$	cr-shft$_{bld}$	$k_{tbc,bld}$	$t_{tbc,bld}$
>1σ	24	2	7	17
>2σ	10	1	1	4
>3σ	4	0	0	0

Table A.5: Number of salvaged engine non-conformances relative to oxidation indicator 1 by means of single-factor tolerancing.

Finite Element Simulations

Tolerance	# of Salvaged Engines			
	$T_{41,eng}$	$\Delta RTDF_{eng}$	$W_{41,eng}$	$T_{3,eng}$
>1σ	35	17	15	18
>2σ	5	2	1	3
>3σ	0	0	0	1

Tolerance	# of Salvaged Engines				
	$D_{SS,LE,bld}$	$D_{PS,LE,bld}$	$D_{PS,CN,bld}$	$D_{PS,TE,bld}$	$m_{cool,bld}$
>1σ	2	-1	0	21	13
>2σ	-1	0	1	7	2
>3σ	0	0	0	1	1

Tolerance	# of Salvaged Engines			
	$k_{sub,bld}$	cr-shft$_{bld}$	$k_{tbc,bld}$	$t_{tbc,bld}$
>1σ	17	0	6	11
>2σ	8	0	1	2
>3σ	3	0	0	0

Fractional-Factorial Response Surface

Tolerance	# of Salvaged Engines			
	$T_{41,eng}$	$\Delta RTDF_{eng}$	$W_{41,eng}$	$T_{3,eng}$
>1σ	35	17	15	18
>2σ	5	2	1	3
>3σ	0	0	0	1

Tolerance	# of Salvaged Engines				
	$D_{SS,LE,bld}$	$D_{PS,LE,bld}$	$D_{PS,CN,bld}$	$D_{PS,TE,bld}$	$m_{cool,bld}$
>1σ	2	-1	0	21	N/A
>2σ	-1	0	1	7	N/A
>3σ	0	0	0	1	N/A

Tolerance	# of Salvaged Engines			
	$k_{sub,bld}$	cr-shft$_{bld}$	$k_{tbc,bld}$	$t_{tbc,bld}$
>1σ	17	0	6	11
>2σ	8	0	1	2
>3σ	3	0	0	0

One-Factor-at-a-Time Response Surface

Tolerance	# of Salvaged Engines			
	$T_{41,eng}$	$\Delta RTDF_{eng}$	$W_{41,eng}$	$T_{3,eng}$
>1σ	34	17	15	17
>2σ	5	2	1	3
>3σ	0	0	0	1

Tolerance	# of Salvaged Engines				
	$D_{SS,LE,bld}$	$D_{PS,LE,bld}$	$D_{PS,CN,bld}$	$D_{PS,TE,bld}$	$m_{cool,bld}$
>1σ	4	1	3	22	N/A
>2σ	0	0	1	7	N/A
>3σ	0	0	0	1	N/A

Tolerance	# of Salvaged Engines			
	$k_{sub,bld}$	cr-shft$_{bld}$	$k_{tbc,bld}$	$t_{tbc,bld}$
>1σ	20	0	7	14
>2σ	10	1	1	4
>3σ	4	0	0	0

Appendix B

Oxidation Indicator 2 Summary

B.1 One-Factor-at-a-Time Response Surface

Table B.1: Oxidation indicator 2 response terms, section 3 $T_{average,PS}$ (screening FEM).

Constant:

	Effect (K)
β_0	+1165.149

Linear Terms:

	β_i **(K)**
$T_{41,eng}$	+3.589
$\Delta RTDF_{eng}$	+1.271
$W_{41,eng}$	+0.231
$T_{3,eng}$	+1.106
$D_{SS,LE,bld}$	-0.307
$D_{PS,LE,bld}$	-0.588
$D_{PS,CN,bld}$	-1.311
$D_{PS,TE,bld}$	-4.884
$k_{sub,bld}$	-0.306
$coreshift_{bld}$	+1.101
$k_{tbc,bld}$	+1.346
$t_{tbc,bld}$	-2.691

B.2 Fractional-Factorial Response Surface

Table B.2: Oxidation indicator 2 response terms, section 3 $T_{average,PS}$ (RS FEM).

Linear Terms:

	β_i **(K)**
$T_{41,eng}$	+3.591
$\Delta RTDF_{eng}$	+1.272
$W_{41,eng}$	+0.231
$T_{3,eng}$	+1.105
$D_{SS,LE,bld}$	-0.307
$D_{PS,LE,bld}$	-0.587
$D_{PS,CN,bld}$	-1.309
$D_{PS,TE,bld}$	-4.884
$k_{sub,bld}$	-0.306
$coreshift_{bld}$	+1.100
$k_{tbc,bld}$	+1.345
$t_{tbc,bld}$	-2.692

Second Order Terms:

$\beta_{i,j}$ **(K)**	$T_{41,eng}$	$\Delta RTDF_{eng}$	$T_{3,eng}$	$D_{SS,LE,bld}$	$D_{PS,LE,bld}$	$D_{PS,CN,bld}$	$D_{PS,TE,bld}$	$k_{sub,bld}$	$coreshift_{bld}$	$k_{tbc,bld}$	$t_{tbc,bld}$
$T_{41,eng}$	-9.41e-05	+8.26e-14	-2.66e-04	-2.45e-03	-4.60e-03	-1.00e-02	-3.62e-02	-1.73e-03	+8.47e-03	+9.92e-03	-1.98e-02
$\Delta RTDF_{eng}$	-	-9.41e-05	-1.56e-05	-6.45e-04	-1.54e-03	-3.57e-03	-1.49e-02	-1.30e-03	+3.17e-03	+4.15e-03	-8.29e-03
$T_{3,eng}$	-	-	+4.06e-04	+6.21e-04	+1.18e-03	+2.49e-03	+8.48e-03	+1.02e-04	-1.85e-03	-2.27e-03	+4.53e-03
$D_{SS,LE,bld}$	-	-	-	+1.91e-03	+9.01e-03	+9.53e-03	+1.29e-02	-1.82e-03	+5.56e-03	+3.28e-04	-5.98e-04
$D_{PS,LE,bld}$	-	-	-	-	+4.91e-03	+1.15e-02	+1.54e-02	+1.44e-03	+2.69e-02	-3.05e-04	+6.13e-04
$D_{PS,CN,bld}$	-	-	-	-	-	+1.94e-02	+6.53e-02	-7.99e-03	+2.39e-02	-1.07e-03	+2.15e-03
$D_{PS,TE,bld}$	-	-	-	-	-	-	+1.66e-01	-1.87e-02	-4.49e-02	+6.27e-03	-1.25e-02
$k_{sub,bld}$	-	-	-	-	-	-	-	+1.04e-02	+2.66e-02	+2.47e-03	-4.95e-03
$coreshift_{bld}$	-	-	-	-	-	-	-	-	+2.94e-02	+2.46e-04	-5.16e-04
$k_{tbc,bld}$	-	-	-	-	-	-	-	-	-	-4.06e-02	+7.26e-02
$t_{tbc,bld}$	-	-	-	-	-	-	-	-	-	-	+1.69e-02

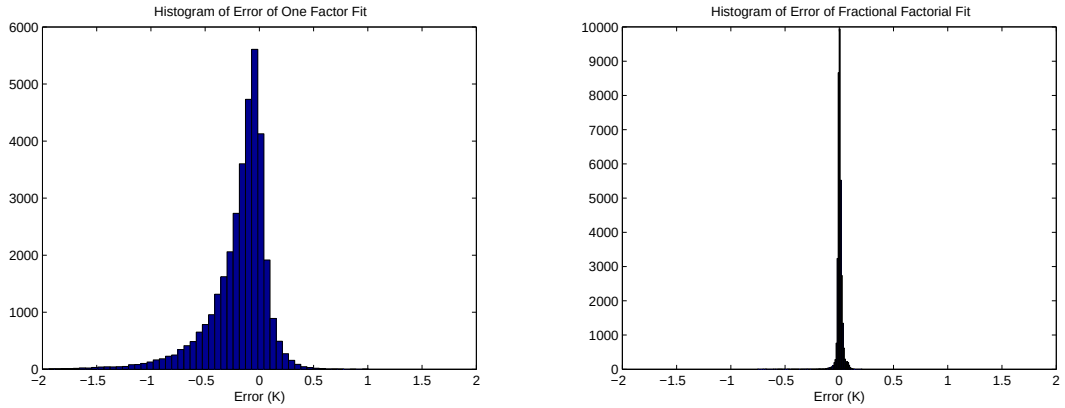

(a) (b)

Figure B-1: Histogram of error of (a) one-factor-at-a-time; (b) fractional-factorial response surfaces relative to finite element oxidation indicator 2 solutions.

Table B.3: Statistics of error of response surfaces relative to finite element oxidation indicator 2 solutions.

type of response surface	$\mu(error)$	$\sigma(error)$
one-factor-at-a-time	-0.190	0.290
fractional-factorial	0.003	0.028

B.3 Monte Carlo Simulations

Table B.4: Number of conclusive engine non-conformances for oxidation indicator 2.

Finite Element Simulations

Range	# (Conclusive) Engine NC Given BR			
	$T_{41,eng}$	$\Delta RTDF_{eng}$	$W_{41,eng}$	$T_{3,eng}$
>1σ	22	19	10	12
>2σ	4	3	1	1
>3σ	0	0	0	1

Range	# Conclusive Engine NC Given BR				
	$D_{SS,LE,bld}$	$D_{PS,LE,bld}$	$D_{PS,CN,bld}$	$D_{PS,TE,bld}$	$m_{cool,bld}$
>1σ	13	8	13	47	43
>2σ	2	2	4	35	24
>3σ	1	0	0	10	9

Range	# Conclusive Engine NC Given BR			
	$k_{sub,bld}$	cr-shft$_{bld}$	$k_{tbc,bld}$	$t_{tbc,bld}$
>1σ	5	9	20	31
>2σ	0	2	4	10
>3σ	0	0	0	2

Fractional-Factorial Response Surface

Range	# (Conclusive) Engine NC Given BR			
	$T_{41,eng}$	$\Delta RTDF_{eng}$	$W_{41,eng}$	$T_{3,eng}$
>1σ	21	18	10	12
>2σ	4	2	1	1
>3σ	0	0	0	1

Range	# Conclusive Engine NC Given BR				
	$D_{SS,LE,bld}$	$D_{PS,LE,bld}$	$D_{PS,CN,bld}$	$D_{PS,TE,bld}$	$m_{cool,bld}$
>1σ	13	8	13	47	44
>2σ	2	2	4	36	25
>3σ	1	0	0	11	9

Range	# Conclusive Engine NC Given BR			
	$k_{sub,bld}$	cr-shft$_{bld}$	$k_{tbc,bld}$	$t_{tbc,bld}$
>1σ	5	10	19	30
>2σ	0	3	3	10
>3σ	0	0	0	2

One-Factor-at-a-Time Response Surface

Range	# (Conclusive) Engine NC Given BR			
	$T_{41,eng}$	$\Delta RTDF_{eng}$	$W_{41,eng}$	$T_{3,eng}$
>1σ	23	18	12	13
>2σ	5	3	2	1
>3σ	0	0	0	1

Range	# Conclusive Engine NC Given BR				
	$D_{SS,LE,bld}$	$D_{PS,LE,bld}$	$D_{PS,CN,bld}$	$D_{PS,TE,bld}$	$m_{cool,bld}$
>1σ	13	8	13	45	N/A
>2σ	2	2	4	33	N/A
>3σ	0	0	0	7	N/A

Range	# Conclusive Engine NC Given BR			
	$k_{sub,bld}$	cr-shft$_{bld}$	$k_{tbc,bld}$	$t_{tbc,bld}$
>1σ	5	9	21	33
>2σ	0	2	4	11
>3σ	0	0	0	2

Table B.5: Number of salvaged engine non-conformances relative to oxidation indicator 2 by means of single-factor tolerancing.

Finite Element Simulations

Tolerance	# of Salvaged Engines			
	$T_{41,eng}$	$\Delta RTDF_{eng}$	$W_{41,eng}$	$T_{3,eng}$
>1σ	21	16	7	10
>2σ	4	3	0	0
>3σ	0	0	0	1

Tolerance	# of Salvaged Engines				
	$D_{SS,LE,bld}$	$D_{PS,LE,bld}$	$D_{PS,CN,bld}$	$D_{PS,TE,bld}$	$m_{cool,bld}$
>1σ	4	3	10	47	43
>2σ	1	1	2	35	24
>3σ	1	0	0	10	9

Tolerance	# of Salvaged Engines			
	$k_{sub,bld}$	cr-shft$_{bld}$	$k_{tbc,bld}$	$t_{tbc,bld}$
>1σ	-4	4	17	24
>2σ	0	1	3	7
>3σ	0	0	0	2

Fractional-Factorial Response Surface

Tolerance	# of Salvaged Engines			
	$T_{41,eng}$	$\Delta RTDF_{eng}$	$W_{41,eng}$	$T_{3,eng}$
>1σ	20	15	7	10
>2σ	4	2	0	0
>3σ	0	0	0	1

Tolerance	# of Salvaged Engines				
	$D_{SS,LE,bld}$	$D_{PS,LE,bld}$	$D_{PS,CN,bld}$	$D_{PS,TE,bld}$	$m_{cool,bld}$
>1σ	4	3	10	47	N/A
>2σ	1	1	2	36	N/A
>3σ	1	0	0	11	N/A

Tolerance	# of Salvaged Engines			
	$k_{sub,bld}$	cr-shft$_{bld}$	$k_{tbc,bld}$	$t_{tbc,bld}$
>1σ	-4	5	16	23
>2σ	0	2	2	7
>3σ	0	0	0	2

One-Factor-at-a-Time Response Surface

Tolerance	# of Salvaged Engines			
	$T_{41,eng}$	$\Delta RTDF_{eng}$	$W_{41,eng}$	$T_{3,eng}$
>1σ	22	15	9	11
>2σ	5	3	1	0
>3σ	0	0	0	1

Tolerance	# of Salvaged Engines				
	$D_{SS,LE,bld}$	$D_{PS,LE,bld}$	$D_{PS,CN,bld}$	$D_{PS,TE,bld}$	$m_{cool,bld}$
>1σ	5	4	10	45	N/A
>2σ	1	0	2	33	N/A
>3σ	0	0	0	7	N/A

Tolerance	# of Salvaged Engines			
	$k_{sub,bld}$	cr-shft$_{bld}$	$k_{tbc,bld}$	$t_{tbc,bld}$
>1σ	-3	4	19	26
>2σ	0	0	3	8
>3σ	0	0	0	2

Bibliography

[1] SAE Interntational. http://www.sae.org/aeromag/techinnovations/1298t10.htm.

[2] Carroll Vincent Sidwell. *On the Impact of Variability and Assembly on Turbine Blade Cooling Flow and Oxidation Life.* Doctor of philosophy dissertation, Massachusetts Institute of Technology, Department of Aeronautics and Astronautics, June 2004.

[3] MIT Open Course Ware. http://ocw.mit.edu/ans7870/16/16.unified/propulsions04/unifiedpropulsion3/unifiedpropulsion3.htm.

[4] Bernard L. Koff. Gas turbine technology evolution - a designer's perspective. AIAA-2003-2722, AIAA/ICAS International Air and Space Symposium and Exposition.

[5] Je-Chin Han, Sandip Dutta, and Srinath V. Ekkad. *Gas Turbine Heat Transfer and Cooling Technology.* Taylor and Francis, New York, NY, 2000.

[6] Matthias Voigt, Roland Mücke, Konrad Vogeler, and Michael Oevermann. Probabilistic lifetime analysis for turbine blades based on a combined direct monte carlo and response surface approach. GT2004-53439, 2004 ASME Turbo Expo.

[7] Irem Y. Tumer and Anupa Bajwa. Learning about how aircraft engines work and fail. AIAA-99-2850.

[8] Robert Kingston-Rolls Royce. Personal communication 2005.

[9] Rolls Royce. http://www.rolls-royce.com/service/civil/totalcare/default.jsp.

[10] R. Haimes and A. Merchant. The synergistic use of cad for tightly coupled analysis and design. AIAA-2005-4986.

[11] R. Craig McClung, Henry L. Bernstein, Janet P. Buckingham, James M. Allen, and George L. Touchton. Probabilistic analyses of industrial gas turbine durability. 93-GT-427.

[12] Roland Mücke. A probabilistic desing approach to lifetime prediction for turbine blades. European Congress on Computational Methods in Applied Sciences and Engineering, ECCOMAS 2000.

[13] Vitali V. Volovoi, Mark Waters, and Dimitri N. Mavris. Comparative assessment of direct and indirect probabilistic methods for thermomechanical analyiss of structural components in gas turbines. GT2003-38510, 2003 ASME Turbo Expo.

[14] Stefan Reh, Tamas Palfi, and Noel N. Nemeth. Probabilistic analysis techniques applied to lifetime reliability estimation of ceramics. JANNAF 39th Combustion Subcommittee, 27th Airbreathing Propulsion, 21st Propulsion Systems Hazards Committee, and 3rd Modeling and Simulation Subcommittee Joint Meeting, December 2003. Available from Chemical Propulsion Information Agency.

[15] Vince Sidwell and David Darmofal. The impact of blade-to-blade flow variability on turbine blade coolin performance. ASME Journal of Turbomachinery, October 2005 Vol. 127.

[16] Francesco Martelli, Francesco Montomoli, Paolo Adami, and Stefania Della Gatta. Conjugate heat transfer modelling in film cooled blades. GT2004-53177, 2004 ASME Turbo Expo.

[17] Frank P. Incropera and David P. DeWitt. *Fundamentals of Heat and Mass Transfer: Fifth Edition*. John Wiley and Sons, New York, NY, 2002.

[18] Robert Norton-Rolls Royce. Personal communication 2005.

[19] Alexander Karl-Rolls Royce. Personal communication 2005.

[20] Rupert Taylor-Rolls Royce. Personal communication 2005.

[21] Hubert W. Lilliefors. On the kolmogorov-smirnov test for normality with mean and variance unknown. volume 62 of *Journal of the American Statistical Association*, pages 399–402, 1967.

[22] J.F. Monahan. *Numerical Methods of Statistics*. Cambridge University Press, 2001.

[23] ANSYS Inc. Ansys release 8.0 documentation. 2003.

[24] Raymond H. Myers and Douglas C. Montgomery. *Response Surface Methodology: Process and Product Optimization Using Designed Experiments*. John Wiley and Sons, New York, NY, 1995.

[25] Douglas C. Montgomery. *Design and Analysis of Experiments, Fourth Edition*. John Wiley and Sons, New York, NY, 1997.

[26] R.E. Walpole, R. H. Myers, and S.L. Myers. *Probability and Statistics for Engineers and Scientists: Sixth Edition*. Prentice Hall, Upper Saddle River, NJ, 1998.